JOTCS A
Journal of the Turkish Chemical Society
Section: A
Chemistry

TURKISH CHEMICAL SOCIETY

Magnetic Molecularly Imprinted Polymer Synthesis and Application for Selective Separation of Quercetin

Şeyda Karaman Ersoy[1*], Merve Akyüz[2], Kevser Sözgen Başkan[2]

[1]Fenerbahçe University, Faculty of Pharmacy, Department of Analytical Chemistry, İstanbul, 34758, Turkey.
[2]İstanbul University-Cerrahpaşa, Faculty of Engineering, Department of Chemistry, İstanbul, 34320, Turkey.

Abstract: Quercetin (QUE) is the most active compound in the flavone family, commonly found in the leaves, fruits, and flowers of many plants. The separation of QUE from various plant matrices has been a key research area due to its antioxidant, anti-inflammatory, antiviral, and antitumor properties. In this study, the conditions for synthesizing MMIPs and their use in QUE recovery were examined. Iron (II) chloride tetrahydrate ($FeCl_2{\cdot}4H_2O$) and iron (III) chloride hexahydrate ($FeCl_3{\cdot}6H_2O$) were used to prepare magnetic nanoparticles, and Fe_3O_4 was synthesized. Tetraethyl orthosilicate (TEOS) was used to coat the resulting Fe_3O_4 surface with silica. [3-(methacryloxy)propyl] trimethoxysilane (γ-MPS) was used to functionalize the surface of the formed Fe_3O_4@TEOS structure. The synthesis was carried out using QUE as the template molecule; tetrahydrofuran (THF), ethanol (EtOH), and a solvent mixture of acetone and acetonitrile (ACN) (3:1, v/v) served as porogen solvents; acrylamide (AM), methacrylic acid (MAA), and 4-vinylpyridine (4-VP) were used as functional monomers; ethylene glycol dimethacrylate (EDMA) served as the cross-linker, and 2,2'-azobisisobutyronitrile (AIBN) was used as the initiator at different molar ratios (T:M:CrL, 1:4:20, 1:8:20, and 1:8:40). The recognition and selectivity properties of these polymers were evaluated based on absorbance values at 370 nm obtained through equilibrium assays, which used QUE solutions prepared in THF, ACN, and 50% (v/v) EtOH solvent mixtures at different ratios. It was established that the magnetic imprinted polymer prepared with a 50% (v/v) EtOH solvent mixture and molar ratios of 1:8:40 (QUE:4-VP:EDMA) exhibited the highest adsorption capacity and imprinting factor. Using the prepared QUE-MMIP, QUE was recovered with 33% efficiency from red onion peel extract.

Keywords: Quercetin, Magnetic molecularly imprinted polymer, Red onion peel.

Submitted: January 2, 2025. **Accepted:** June 10, 2025.

Cite this: Karaman Ersoy Ş, Akyüz M, Sözgen Başkan K. Magnetic Molecularly Imprinted Polymer Synthesis and Application for Selective Separation of Quercetin. JOTCSA. 2025;12(3): 155-168.

DOI: https://doi.org/10.18596/jotcsa.1608405

***Corresponding author's E-mail:** seyda.ersoy@fbu.edu.tr

1. INTRODUCTION

In recent years, there has been a growing interest in plant antioxidants that can be used in their unmodified form as natural food preservatives, replacing synthetic substances. One of these substances, Quercetin (QUE), a flavonol found in fruits and vegetables, is a food ingredient with proven beneficial effects on health and is widely used in pharmaceutical, cosmetic, and nutraceutical products. It has been reported that quercetin is abundant in onion and apple species, and it is also found in onion peels approximately 77 times more than the edible part (1-4).

However, the selective extraction of quercetin from natural sources remains a significant challenge due to the complexity of plant matrices and the presence of structurally similar phenolic compounds. Conventional extraction methods often lack the specificity required to isolate QUE, resulting in low purity and yield efficiently. Therefore, there is a pressing need for advanced materials capable of selectively recognizing and isolating target molecules such as QUE from complex mixtures.

The selective separation of QUE and other bioactive compounds from the natural matrix cannot be achieved with traditional extraction methods. Effective isolation of target analytes from complex sample matrices depends on using highly efficient extraction materials that can interact selectively with them (5-7). Many studies in the literature demonstrate that materials suitable for this purpose

can be prepared using molecular imprinting technology (6). Molecularly imprinted polymers (MIPs), produced by this technique, contain many cavities that match the shape, size, and chemical functionality of the template molecules. In other words, MIPs are materials with predefined selectivity for target molecules. This design can be explained by analogy, such as the "lock and key model" described by Emil Fischer over a century ago (8). Besides many other applications, MIPs, which are important as molecular recognition tools in analytical chemistry, are used to aid in the detection of amino acids, peptides, proteins, nucleotide derivatives, toxic substances including pesticide residues, antibiotics, artificial hormones, and food adulterants (9,10). MIPs are also valuable for identifying and extracting plant compounds (8). There are studies on using MIPs for the selective extraction, determination, and preconcentration of quercetin (11-14).

Molecularly imprinted polymers have a wide range of applications because of their high affinity and selectivity for the template molecule, their ability to retain recognition ability for a long time, high physical and chemical stability, durability, and ease of preparation. Besides the advantages of MIPs, magnetically imprinted polymers (MMIPs), which acquire magnetic properties, are also used for similar purposes. Compared to traditional solid supports, magnetic materials offer several superior features, such as a high surface-to-volume ratio, rapid and effective binding with the template molecule, and high magnetic susceptibility. Additionally, the MMIPs with the target molecule attached can be easily separated from the environment using external magnets without filtration or centrifugation (15,16). The MMIP consists of a magnetic component (such as nickel, -Fe_2O_3, Fe_3O_4, NiO, and their alloys) and an MIP component. Among magnetic materials, Fe_3O_4 is the most commonly used because it is easy to produce, has low toxicity, and has abundant hydroxyl groups that enable surface modifications (17). The synthesis of MMIPs mainly involves three steps: first, the production of magnetic nanoparticles; second, the modification of the magnetic core-shell surface; and third, the synthesis of the MIP with the target template molecule and coating of the core with this polymer. To make the MMIP ready for use, the template molecule must be removed.

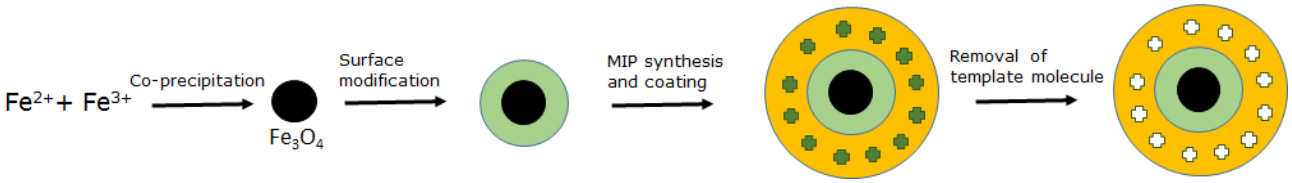

Figure 1: Schematic diagram of magnetic molecularly imprinted polymer (MMIP) synthesis.

MMIPs have been used for the selective separation of various plant-derived bioactive compounds, including QUE (7,15,16,18,19). The synthesis of magnetic MIPs for recovering bioactive compounds from natural samples is a relatively new research area in our country, with limited studies available. This study presents the synthesis of a novel QUE-imprinted MMIP and its application for QUE recovery from a natural matrix. QUE, a prominent flavonol, was chosen as the template molecule for imprinting. Bulk polymerization was selected for QUE-MMIP synthesis because of its ability to produce uniform structures. The optimal functional monomer, porogen solvent, and T:M:CrL molar ratio were determined for MMIP synthesis. A magnetic non-imprinted polymer (MNIP) was also synthesized under the same conditions as MMIP. Fourier Transform Infrared-Attenuated Total Reflectance (FTIR-ATR) spectroscopy was used to analyze structural differences between QUE-MMIP and MNIP. The static and theoretical adsorption capacities of QUE-MMIP were evaluated using Freundlich and Langmuir isotherms. Selectivity tests were conducted with rutin (RT), chlorogenic acid (CLA), vanillic acid, and gallic acid (GA) standards. For QUE-MMIP applications, red onion peel extract—known for its high QUE content—was used as a natural sample. Adsorption studies were performed with batch tests, and the results were analyzed by HPLC-PDA. This work reports the development of a novel magnetic molecularly imprinted polymer (MMIP) for selective quercetin extraction, offering improved adsorption capacity, high selectivity, and rapid magnetic separation, contributing to advancements in natural product isolation techniques.

2. EXPERIMENTAL SECTION

2.1. Chemicals

The following chemicals and solvents of analytical reagent grade were supplied from the indicated sources: Vanillic acid (VA; ≥99 % purity), gallic acid (GA; ≥98 % purity), chlorogenic acid (CLA; 98 % purity), acrylamide (AA; ≥99.9% purity) (Fluka, Steinheim, Germany); methanol (MeOH; gradient grade, ≥99.9 % purity), acetonitrile (ACN; gradient grade, ≥99.9 % purity), iron(II) chloride tetrahydrate ($FeCl_2.4H_2O$;≥99%), iron(III) chloride hexahydrate ($FeCl_3.6H_2O$; ≥99% purity), 3-(methacryloxy)propyl trimethoxysilane (γ-MPS; ≥98% purity), tetraethyl orthosilicate (TEOS; reagent grade, ≥99.0% purity), ammonia (NH_3; anhydrous, ≥99.95% purity) (Sigma-Aldrich, Steinheim, Germany); rutin hydrate (RT; ≥94 purity) (Sigma, Steinheim, Germany); quercetin (QUE; ≥95 purity), 4-vinylpyridine (4-VP; ≥95 purity), methacrylic acid (MAA; ≥99% purity), ethylene glycoldimethacrylate (EDMA; ≥98% purity; cross-linking reagent polymerization reactions), 2,2-azobisisobutyronitrile (AIBN; ≥98%; free radical initiator) (Aldrich, Steinheim, Germany); *o*-phosphoric acid (≥85% purity);ethanol (EtOH; suitable for HPLC; ≥99.99%), tetrahydrofuran (THF; suitable for HPLC; (≥99.9% purity), acetone (ideal for HPLC, ≥99.9% purity)(Merck, Darmstadt, Germany). All the chemicals were of analytical grade.

2.2. Instruments

An HPLC system (Waters Breeze 2, Milford, MA, USA) equipped with a PDA detector (Waters 2998), a binary gradient pump (Waters 1525), and a Zorbax Eclipse XDB C18 column (4.6 mm x 250 mm x 5 µm) was used for chromatographic analyses. Data acquisition was performed using Empower PRO (Waters Associates, Milford, MA). Absorbances were measured with a Varian Cary 1E UV–Vis spectrophotometer (Sydney, Australia) using matched quartz semi-micro cuvettes of 1.4 mL volume and a Daihan HS-30D mechanical mixer (South Korea). Multi Bio RS-24 shaker (Latvia) for batch testing. A Witeg water bath was used for incubation. The evaporation of the extracting solvent was performed with a Büchi R210/215 rotary evaporator (Flawil, Switzerland). Additional equipment included an Isolab vacuum pump (İstanbul, Turkey), an Agilent 12-port SPE system (Waldbronn, Germany), and a Daihan vacuum oven (South Korea). Pure water for all solutions was obtained from a Millipore Simpak1 Synergy185 ultrapure water system (France).

2.3. Development of HPLC Method for The Analysis of Phenolic Compounds

In this study, to evaluate the usability of the synthesized MMIP for the selective separation of QUE from phenolic compounds, the analyses were carried out by HPLC method. A new method based on gradient elution was developed using bidistilled water (B) containing 0.2% *o*-H_3PO_4 with MeOH (A) as the mobile phase (Table 1). Flow rate is 1 ml min^{-1}, detection wavelength is 370 nm.

Table 1: HPLC method for the analysis of compounds in the studied samples.

Time	A%	B%	Curve
0-3 min	35	65	6
3-5 min	50	50	6
5-10 min	80	20	6
10-15 min	100	0	6

2.4. Synthesis of Magnetic Molecularly Imprinted Polymers (MMIPs)

In this study, magnetic molecularly imprinted polymers with QUE were synthesized to enable selective separation of QUE and its derivatives within the flavonol group of phenolic compounds. The synthesis of the polymer specific to QUE involved non-covalent interactions conducted in suitable solvent media (such as THF, ACN, or ACN:DMSO), using various molar ratios of template molecule, monomer, and crosslinker (1:4:20, 1:8:20, 1:8:40) under optimal polymerization conditions (in a water bath at 60 °C for 24 hours under N_2). These procedures were also applied to the non-imprinted polymer (without the template molecule, MNIP). The synthesis of magnetic molecularly imprinted polymers involves two main steps: first, the synthesis of magnetic material, and second, the polymerization process.

2.4.1. Synthesis of magnetic material

4.30 g of $FeCl_2.4H_2O$ (iron(II) chloride tetrahydrate) and 11.68 g of $FeCl_3.6H_2O$ (iron(III) chloride hexahydrate) were weighed, and 200 mL of ultrapure water was added. The mixture was stirred mechanically at 80 °C under nitrogen gas at 800 rpm. Fe_3O_4, which is unstable in the presence of O_2 and/or H+ ions, can easily oxidize to Fe_2O_3. To prevent this, precipitation was carried out by adding excess ammonium hydroxide (20). After adding 22 mL of NH_3:H_2O (28%, v/v), stirring continued for 4 hours. The Fe_3O_4 particles were separated using an external magnet, and the upper aqueous phase was discarded, following the method of Chai et al. (21).

2.4.2. Modification of the surface of the magnetic cores

After obtaining Fe_3O_4 magnetite, its surface was coated with a SiO_2 film. The procedure is as follows: First, the magnetic nanoparticles were evenly dispersed in 80% (v/v) MeOH, then 4 mL of NH_3:H_2O (28%, v/v) solution and 3 mL of TEOS were added slowly. The silica-coated magnetic nanoparticles were then separated using an external magnet and washed several times with ultrapure water. The purpose of coating the magnetite cores with SiO_2 is to improve their dispersion in water and prevent agglomeration. Additionally, the SiO_2 shell allows for further modification of the magnetite nanoparticles. In the next step, the surface modification was completed by coating the SiO_2-coated magnetic nanoparticles (Fe_3O_4@SiO_2) with γ-MPS {[3-(methacryloxy)propyl]trimethoxysilane}. For this, the silica-coated nanoparticles were mixed in 40% (v/v) EtOH under a nitrogen gas flow, then 3 mL of γ-MPS was added to the mixture, and stirring continued for 6 hours. After this, it was stirred for an additional hour at 70 °C. The final product, Fe_3O_4@SiO_2@MPS (Figure 2), was washed with EtOH and ultrapure water until the rinse water reached pH 7.0-7.5 and dried for 24 hours in a vacuum oven at 60°C. The use of γ-MPS is because it provides an attachment site for the polymer via its vinyl group (-CH=CH_2) (7).

Figure 2: Synthesis of γ-MPS-SiO_2@Fe_3O_4.

2.4.3. Synthesis of QUE-MMIP and MNIP

2.4.3.1. Selection of the appropriate functional monomer

MMIP synthesis was performed using suspension, ultrasonic, and bulk polymerization methods, with batch test results showing that bulk polymerization was the most effective. Functional monomers 4-VP, AA, and MAA were employed to synthesize both QUE-imprinted and non-imprinted magnetic polymers. To identify the optimal monomer, imprinted polymers were prepared with a template:monomer:cross-linker (T:M:CrL) molar ratio of 1:8:40, while non-imprinted polymers were synthesized without a template molecule, using THF as the solvent.

For QUE-imprinted magnetic polymer synthesis, a solution containing 0.1 mmol QUE and 0.8 mmol monomer in 20 mL of THF was prepared in a sealed tube. Pre-polymerization was started by bubbling N_2 gas through the solution for 10 minutes, followed by a 30-minute incubation in darkness. Next, 100 mg of γ-MPS-SiO_2@Fe_3O_4 was added and mixed for 2 hours. After adding 4 mmol EDMA and 20 mg AIBN, the mixture was sonicated for 15 minutes and then purged with N_2 gas for 10 minutes. Polymerization was completed by sealing the tube and incubating it at 60 °C in a water bath for 24 hours. The polymers were then isolated and dried in a vacuum oven at 60 °C. Template removal was carried out via Soxhlet extraction using MeOH:HAc (8:2, v/v) as the solvent, with spectrophotometric monitoring until absorbance reached zero. Afterward, washes with MeOH and ultrapure water were performed until the pH stabilized between 6.5 and 7.5, followed by vacuum drying at 60 °C. The synthesis of non-imprinted magnetic polymers (MNIPs) followed the same procedure, minus the template molecule. A schematic diagram of the QUE-MMIP synthesis process is shown in Figure 3.

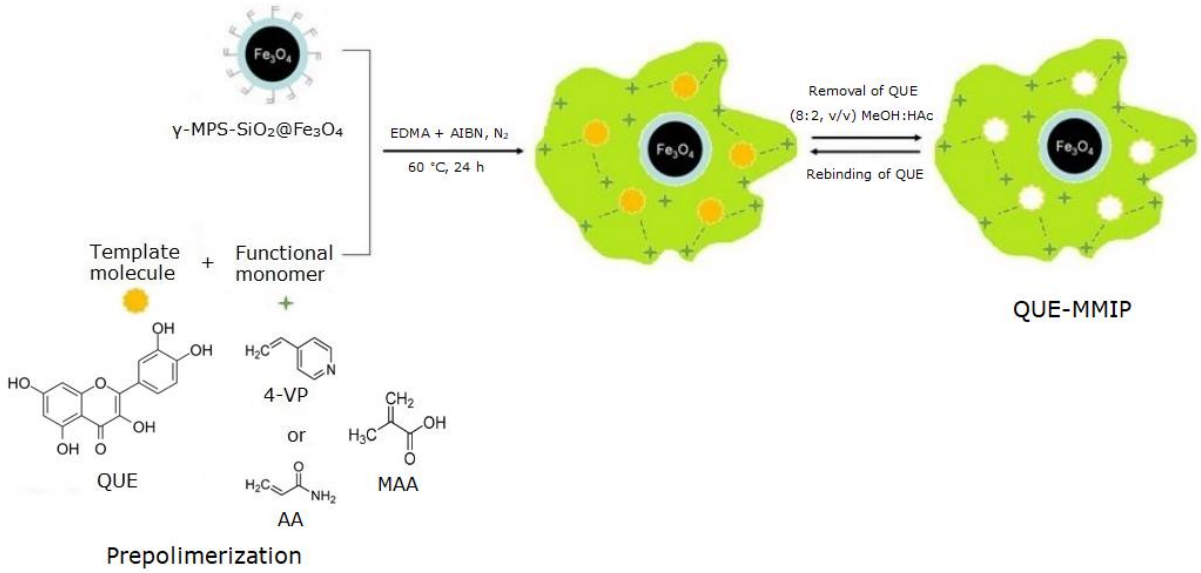

Figure 3: Schematic diagram of QUE-MMIP synthesis.

2.4.3.2. Selection of the appropriate porogen

After identifying 4-VP as the most suitable monomer for QUE-MMIP in the previous section, polymer synthesis was performed using this monomer, but with different solvents or solvent mixtures each time, following the procedure described above. The solvents and solvent mixtures used include acetone:ACN (3:1, v/v), EtOH, acetone, THF:MeOH:H_2O (6:3:1, v/v/v), and THF. To determine the most appropriate porogen, QUE was loaded into the prepared QUE-MMIP using the batch test, and the adsorption efficiency was measured spectrophotometrically.

2.4.3.3. Selection of the appropriate template/monomer/cross-linker ratio

QUE-MMIP syntheses were performed using 4-VP monomer and ethanol as the solvent at molar ratios of 1:8:20, 1:5:40, and 1:8:40 (T:M:CrL). Additionally, polymers were prepared at molar ratios

of 1:8:20, 1:4:20, and 1:8:40 using the same monomer and THF as the solvent. QUE loading was conducted on all prepared polymers with a batch test, and the most suitable molar ratios for the preparation of QUE-MMIP were determined based on the adsorption efficiency values obtained spectrophotometrically.

2.5. Examination of QUE-MMIP Rebinding Parameters

2.5.1. Effect of time on rebinding

To evaluate the effect of time on QUE rebinding, 20 mg of MMIP and MNIP were placed in six separate tubes, each containing 4 mL of a 60 µM QUE solution prepared in 50% (v/v) EtOH. Samples were shaken in a water bath at room temperature for 2, 4, 6, 18, 24, and 48 hours. MMIP was separated using an external magnet, and the remaining QUE concentration was determined by measuring absorbance at 370 nm after filtration through microfilters. The optimal adsorption time was identified based on the adsorption-time graph.

2.5.2. Effect of solvent on rebinding

To investigate the effect of solvent on the rebinding of QUE with MMIPs, loading experiments were conducted using different solvents after the complete removal of QUE from the MMIPs. In these studies, ACN, THF, and 50% (v/v) EtOH solvents were utilized. Solutions of 60 µM QUE prepared in different solvents were added to 20 mg of MMIP and MNIP in each case, and the mixtures were shaken for 2 hours. After separating the polymer with an external magnet, the solutions were filtered, and the optimal loading solvent was determined based on the absorbance measured at a wavelength of 370 nm.

2.5.3. Eff*ect of QUE concentration on rebinding*

To investigate the effect of QUE concentration on the rebinding to QUE-MMIPs, 20 mg of the prepared polymer was weighed and 4 mL of QUE solutions in the concentration range of 20-100 µM prepared in the specified solvent were added. After shaking in a water bath at room temperature for the specified time, MMIPs were separated with an external magnet. The amounts of QUE in the solutions filtered through 1.0/0.45 µm GF/PET micro filters were determined using absorbances at 370 nm wavelength.

2.6. Determination of the Adsorption Properties of QUE-MMIPs

2.6.1. Batch adsorption test

Batch adsorption test was applied with QUE standards prepared at different concentrations for QUE-MMIP and MNIP. 20 mg of the prepared QUE-MMIP and MNIP were weighed and 4 mL of QUE solutions in the 20-80 µM concentration range were added and shaken in a water bath at room temperature for a specific period. After the polymers were separated with the help of an external magnet, the solutions were filtered through 1.0/0.45 µm micro filters. The QUE amounts in the filtrates were determined by using the absorbances at 370 nm.

By analyzing Freundlich and Langmuir isotherms using batch adsorption data, QUE adsorption isotherms were applied to MMIP and MNIP.

For Freundlich Isotherm, MMIP and MNIP adsorption characteristics were assessed. The following equation, {Eq. (1)}, expresses the Freundlich isotherm, the first known relationship explaining the sorption equation. (2) Q_e: Adsorbed QUE amount on polymer (µg/g) C_e: Equilibrium concentration, or the amount of adsorbate in solution at equilibrium (in millimeters), by taking the logarithm of both sides, the equation can be made more linear.

The Freundlich adsorption isotherm is represented as follows in mathematics:

$$Q_e = K_f C_e^{1/n} \qquad \text{(Eqn. 1)}$$

By taking the logarithm of both sides, the equation can be made more linear.

$$\log Q_e = \log K_f + 1/n \log C_e$$

The second most used adsorption isotherm, the Langmuir model, is written as:

$$Q_e = Q_{max}\, b\, C_e/(1 + bC_e) \qquad \text{(Eqn. 2)}$$

$$C_e/Q_e = 1/(Q_{max}\, b) + C_e/Q_{max}$$

Where Q_e is the amount of adsorption (on adsorbent) per unit weight of MMIP at equilibrium (µg/g), b is the Langmuir adsorption equilibrium constant (L/mol), which represents the adsorption energy, and Q_{max} is the theoretical maximum adsorption capacity (µg/g). C_e is the equilibrium or final concentration (µM) of solution after adsorption.

2.6.2. Selectivity experiments

Selectivity tests of QUE-MMIP and MNIP prepared in appropriate molar ratios for some phenolic compounds were performed using rutin (RT) from the flavonol group of flavonoids such as QUE, chlorogenic acid (CLA) from the hydroxycinnamic acid class, gallic acid (GA) and vanillic acid (VA) from the hydroxybenzoic acid class of phenolic acids.

For this purpose, 20 mg of MMIP and MNIP were weighed into separate tubes, and 4 mL of 60 µM phenolic compound solutions were added and shaken in a water bath at room temperature for a certain period. Polymers were separated with a magnet and the spectra of the solutions passed through the microfilter were taken between 200-400 nm. The amount of each compound remaining in the solution was determined by measuring at the wavelength of maximum absorption (λ_{max}). Then, to determine the adsorption status of the above-mentioned compounds in the presence of QUE, a mixture solution containing 60 µM RT, CLA, VA, GA, and QUE in 50% (v/v) EtOH was prepared. The initial and post-polymer treatment concentrations of the mixtures were determined by HPLC method.

2.7. Investigation of the Structures of MMIPs

FTIR-ATR (Fourier Transform Infrared Spectroscopy - Attenuated Total Reflectance) spectra were obtained for QUE-MMIPs and MNIPs prepared under optimal conditions, and their structures were compared.

2.8. Application of QUE-MMIP in Natural Sample

Red onion peels were used as a natural sample containing QUE.

2.8.1. Preparation of onion peel extracts

0.9 g of air-dried onion peel sample was weighed and extracted in three steps with 25 mL of 70% (v/v) MeOH for 60 minutes, 15 mL for 45 minutes, and 10 mL for 15 minutes in the ultrasonic bath. These three extracts were combined, and the final volume was completed to 50 mL. Then, this extract was evaporated in a rotary evaporator under vacuum at 45°C until it reached dryness. The dry residue was then dissolved in a specific volume of the loading solvent.

2.8.2. Application of QUE-MMIP for analysis of red onion peel extract

The extract, which was evaporated to dryness and redissolved in the loading solvent, was first analyzed by HPLC, and QUE content was determined. 4 mL of this extract was taken separately and shaken in a water bath for 2 hours with 20 mg of QUE-MMIP and MNIP. After the polymers were separated with an external magnet, the remaining solutions were passed through the micro filters, and HPLC analysis was performed. The solid QUE-MMIP remaining after filtration was washed with water, 50% (v/v) EtOH and MeOH:HAc (8:2, v/v) were analyzed by HPLC.

3. RESULTS AND DISCUSSION

3.1. Optimization Studies for the Synthesis of QUE-MMIP

3.1.1. Suitable monomer determination

To identify the most suitable monomer for the synthesis of QUE-MMIPs, three different monomers (AAm, MAA, and 4-VP) were used in a 1:8:40 molar ratio T:M:CrL in THF. Polymers were synthesized with and without imprinting. No polymerization occurred in the MAA-based synthesis. Polymers synthesized with AAm and 4-VP were loaded with 60 µM QUE, and it was observed that the polymer synthesized with 4-VP exhibited the best adsorption.

3.1.2. Suitable porogen determination

After determining 4-VP as the most suitable monomer for the QUE-MMIP synthesis, various solvents as porogen, including EtOH, THF, THF:MeOH (6:3:1), acetone, and acetone:ACN (3:1, v/v), were used to synthesize polymers in a 1:8:40 ratio. Polymers without the template molecule were also prepared using the same solvents. Adsorption tests were conducted in batch mode (60 µM QUE), and the imprinting factors (IF) were determined. The results are shown in Table 2.

Table 2: IF values of polymers synthesized in a 1:8:40 ratio using different porogens.

Porogen	Polymer	Adsorption amount of QUE (µg/g)	Imprinting Factor (IF)
THF	1:8:40 0:8:40	1496 906	1.65
EtOH	1:8:40 0:8:40	1632 1269	1.28
THF:MeOH:H_2O (6:3:1, v/v/v)	1:8:40 0:8:40	Polymer formation occurred; however, the adsorption capacity of the MNIP was found to be higher than that of the MMIP	-
Acetone	1:8:40 0:8:40	No polymer formation	-
Acetone:ACN (3:1, v/v)	1:8:40 0:8:40	No polymer formation	-

3.1.3. Suitable monomer:Cross-linker determination

The ratios used in the synthesis of quercetin-printed magnetic polymers were determined based on similar studies as references. The ratios tested in the quercetin-printed magnetic polymer synthesis were 1:4:20, 1:8:20, and 1:8:40. THF was used as a pore-forming solvent to synthesize both printed and non-printed polymers, and the imprinting factors were determined (Table 3).

Table 3: Comparison of QUE-MMIP and MNIP at different molar composition ratios.

Molar ratio	Adsorption Amount of QUE (µg/g)	Imprinting Factor (IF)
1:8:40 0:8:40	1496 906	1.65
1:8:20 0:8:20	423 287	1.47
1:4:20 0:4:20	695 453	1.53

Based on the imprinting factor values, the most optimal molar ratio for QUE-MMIP was determined to be 1:8:40.

3.2. Investigation of QUE-MMIP Rebinding Parameters

3.2.1. Effect of time on rebinding

20 mg of 1:8:40 QUE-MMIP and MNIP polymers were weighed into five separate tubes, to which 4 mL of a 60 µM QUE solution prepared in a 50% EtOH (v/v) solvent mixture was added. The samples were incubated at room temperature, with a shaking speed of 250 rpm, in a water bath for 2, 4, 6, 18, and 24 hours. The amount of adsorbed QUE was calculated from the absorbance measurements at a wavelength of 370 nm. The measured value at 2 hours was considered sufficient, as the difference in retention between MMIP and MNIP stabilized at that point.

3.2.2. Effect of solvent on rebinding

20 mg of 1:8:40 QUE-MMIP and MNIP polymers were weighed, and 4 mL of 60 µM QUE solutions prepared in THF, ACN, and 50% EtOH (v/v) solvents were added to each. The samples were incubated at room temperature for 2 hours, with a shaking speed of 250 rpm, in a water bath. The amount of adsorbed QUE was calculated based on absorbance measurements at a wavelength of 370 nm. According to the obtained data, the highest adsorption value was determined with 50% (v/v) EtOH.

3.2.3. Effect of T:M:CrL ratio

To investigate the effect of QUE concentration on the polymer's binding capacity, solutions prepared at different concentrations (20-140 µM) in 50% EtOH (v/v) were added to 20 mg of QUE-MMIP and MNIP polymers, and batch testing was performed. The amounts of QUE retained by QUE-MMIP and MNIP, as well as the binding factor (BF) values determined based on concentration, are presented in Table 4.

Table 4: The IF values determined as a result of the adsorption of QUE solutions at different concentrations by MMIP and MNIP.

QUE concentration (µM)	Adsorption amount of QUE on MMIP (µg/g)	Adsorption amount of QUE on MNIP (µg/g)	IF values
20	352	223	1.57
40	1097	789	1.39
60	1496	906	1.65
80	1890	1453	1.30
100	2183	1666	1.31
120	2200	1734	1.26
140	2434	1987	1.22

3.3. Results of the Adsorption Characteristics of QUE-MMIPs

3.3.1. Batch adsorption test

The Freundlich and Langmuir adsorption isotherms were used to evaluate the adsorption properties of QUE-MMIP and MNIP. For both QUE-MMIP and MNIP, the linear Freundlich adsorption isotherm was plotted by examining the relationship between log Ce and log Qe, as shown in equation 1. The slope of the line and its intercept were used to determine the values of 1/n and log K_f. Figure 4 shows the Freundlich adsorption isotherm.

Table 5 represents the Freundlich adsorption isotherm values for QUE-MMIP and MNIP.

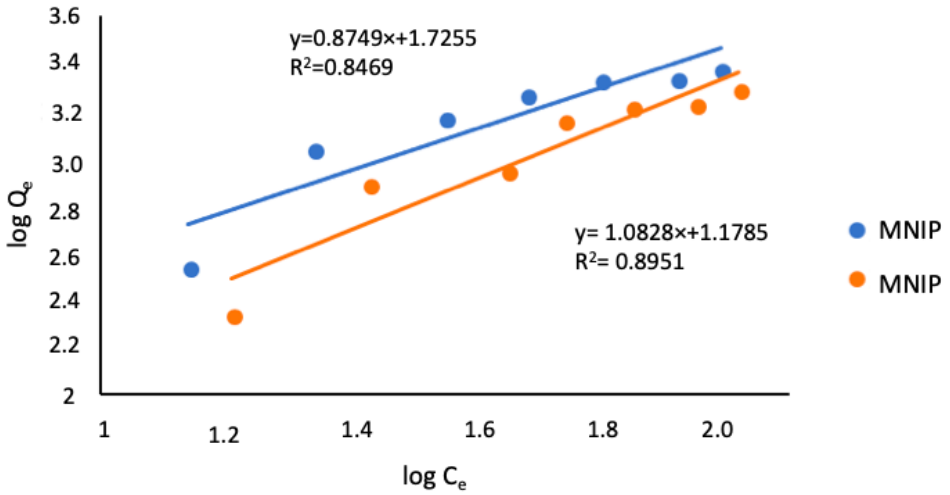

Figure 4: Freundlich Adsorption Isotherm for QUE-MMIP and MNIP (Q_e: the amount of adsorption (on adsorbent) per unit weight of polymer at equilibrium (µg/g), C_e: the equilibrium or final concentration (µM) of solution after adsorption.)

Table 5: Freundlich and Langmuir Adsorption Isotherm values of QUE-MMIP and MNIP (Kf: Freundlich constant; n: Adsorption intensity constant; Q_{max}: Theoretical maximum adsorption capacity; b: Langmuir adsorption equilibrium constant)

Polymer	Freundlich Constants			Langmuir Constants		
	Kf	n	R^2	Qmax	b	R^2
MMIP	53	1.14	0.8469	769	$3.22x10^{-3}$	0.9737
MNIP	15	0.92	0.8951	1000	$2.09x10^{-3}$	0.9000

The adsorption intensity constant (n) of QUE-MMIP was 1.14 (>1), indicating compatibility with the Freundlich isotherm. Langmuir isotherms for QUE-MMIP and MNIP were plotted using C_e and C_e/Q_e values, with Q_{max} and b calculated from the linear plot's slope and intercept. Figure 5 shows the Langmuir isotherm, while Table 5 summarizes adsorption capabilities. The RL value (0.83, RL<1) confirms the suitability of the Langmuir isotherm for QUE-MMIP. Higher correlation coefficients indicate the Langmuir model fits QUE-MMIP adsorption better than the Freundlich model (22,23).

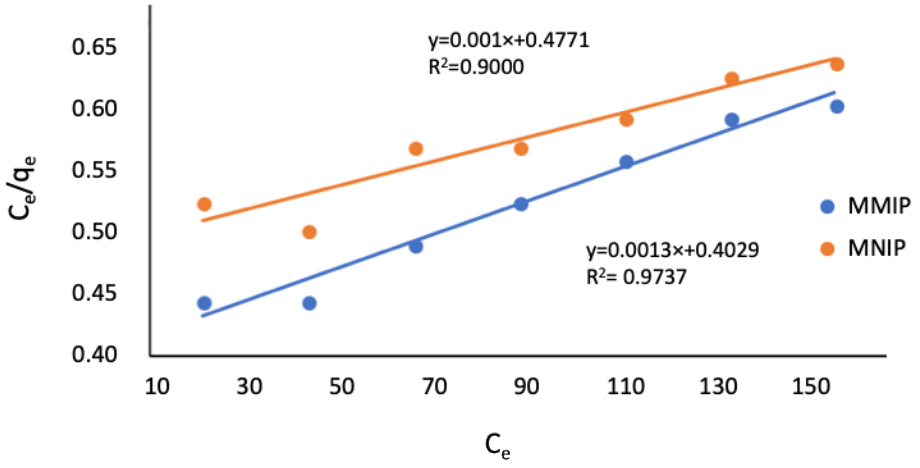

Figure 5: Langmuir Adsorption Isotherms for QUE-MMIP and MNIP (Q_e: the amount of adsorption (on adsorbent) per unit weight of polymer at equilibrium (µg/g), C_e: the equilibrium or final concentration (µM) of solution after adsorption.)

3.4. Investigation of QUE-MMIP and MNIP Structures

The FTIR-ATR spectra of QUE-MMIP and MNIP are shown in Figure 6. For QUE-MMIP, the adsorption bands observed at ~3420 cm^{-1} and ~2950 cm^{-1} correspond to -OH and C-H stretching vibrations, respectively. The vibration observed at 1719 cm^{-1} corresponds to the C=O stretching vibration. The bands observed at ~1450 cm^{-1} and ~1385 cm^{-1} are attributed to $-CH_3$ and $-CH_2$ bending vibrations, respectively. The bands observed at ~1246 cm^{-1} and ~1132 cm^{-1} are interpreted as C-O and Si-O stretching vibrations, respectively (24).

The FTIR-ATR spectra of MMIP and MNIP are nearly identical because, after the removal of the template molecule, the chemical composition of MMIP, is like that of MNIP (25).

3.5. Synthetic Mixture Application to Determine the Selectivity of QUE-MMIP for QUE

4 mL aliquots of each GA, RT, CLA, VA, and QUE were taken from the mixture prepared in 50% (v/v) EtOH at a concentration of 6×10^-5 M and added to 20 mg of QUE-MMIP and MNIP. The samples were shaken in a water bath for 2 hours at room temperature. The mixture was analyzed by HPLC before and after this process. The resulting chromatograms are shown in Figure 7.

As shown in Figure 7, in the synthetic mixture containing 60 µM QUE along with phenolic compounds at the same concentrations, the amount of QUE adsorbed by QUE-MMIP is higher. It was hypothesized that the other components, aside from QUE and RT, bound non-specifically to the polymer without fitting into the template, since they lack a flavonol structure. The low adsorption rate of RT by QUE-MMIP was attributed to its structural difference from QUE, specifically the presence of a rutinoside group, which prevents it from fitting into the template. As depicted in Figure 7, the adsorption of QUE by MNIP was believed to result from non-specific interactions between the -OH groups in its structure and groups on the polymer surface.

3.6. Red Onion Peel Application to Determine the Selectivity of QUE-MMIP for QUE

After evaporation, 1 mL of red onion peel extract in 50% ethanol was diluted to 10 mL, then further diluted at 1:1 and 1:10 ratios. Next, 4 mL of the solution was mixed with 100 mg of MMIP and incubated at 250 rpm for 2 hours. The chromatogram at 370 nm (Figure 8) confirms the presence of quercetin, quercetin glycosides, and kaempferol. The first and third peaks were identified using PDA spectra and literature data (26).

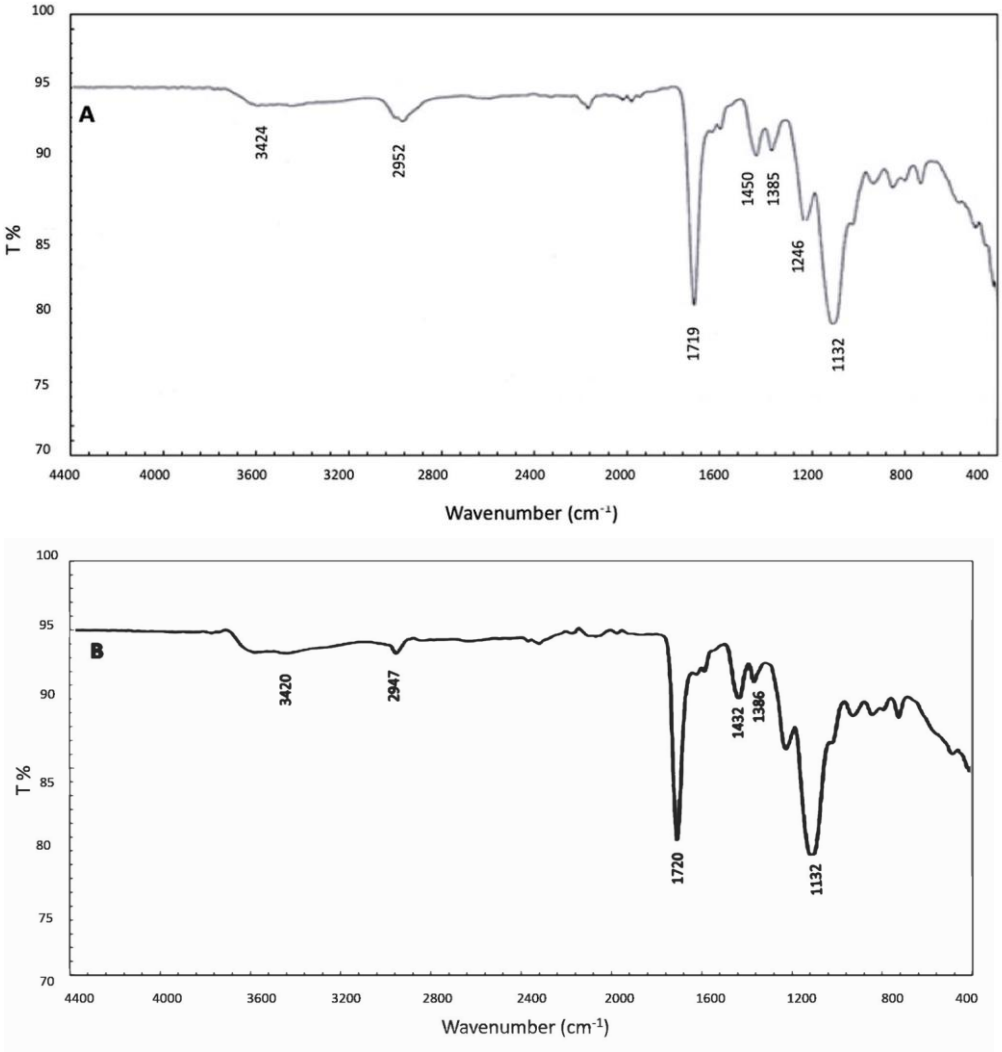

Figure 6: FTIR-ATR spectrum of MMIP (A) and MNIP (B).

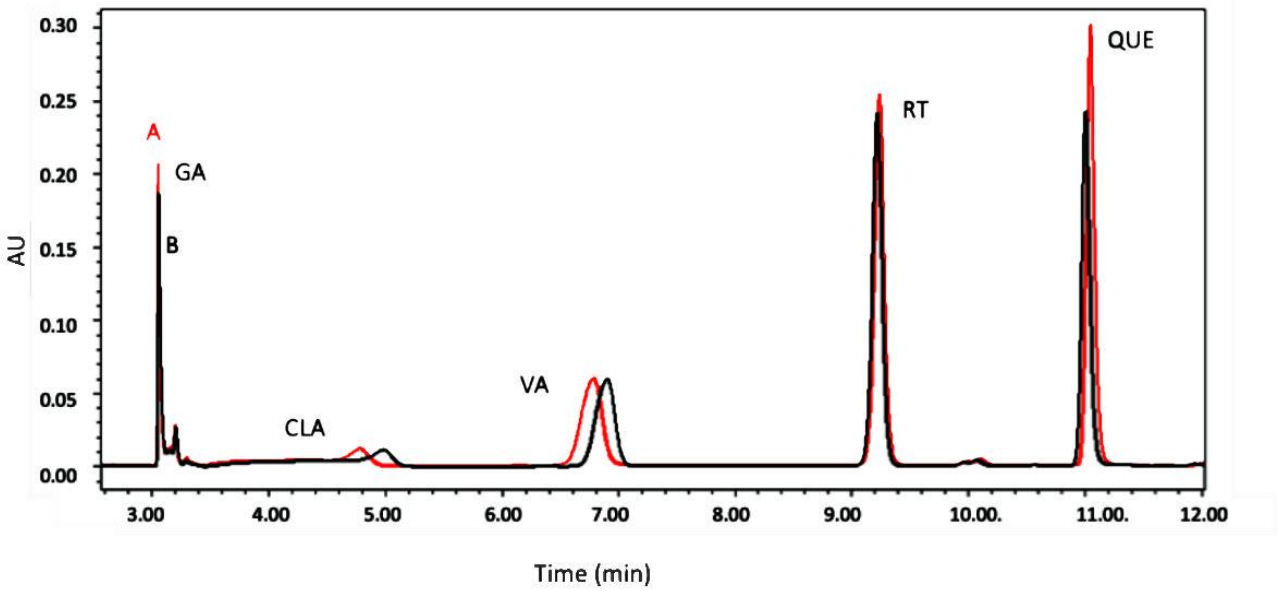

Figure 7: Chromatograms of the synthetic mixture solution before (A) and after (B) treatment with QUE-MMIP (λ = 260 nm).

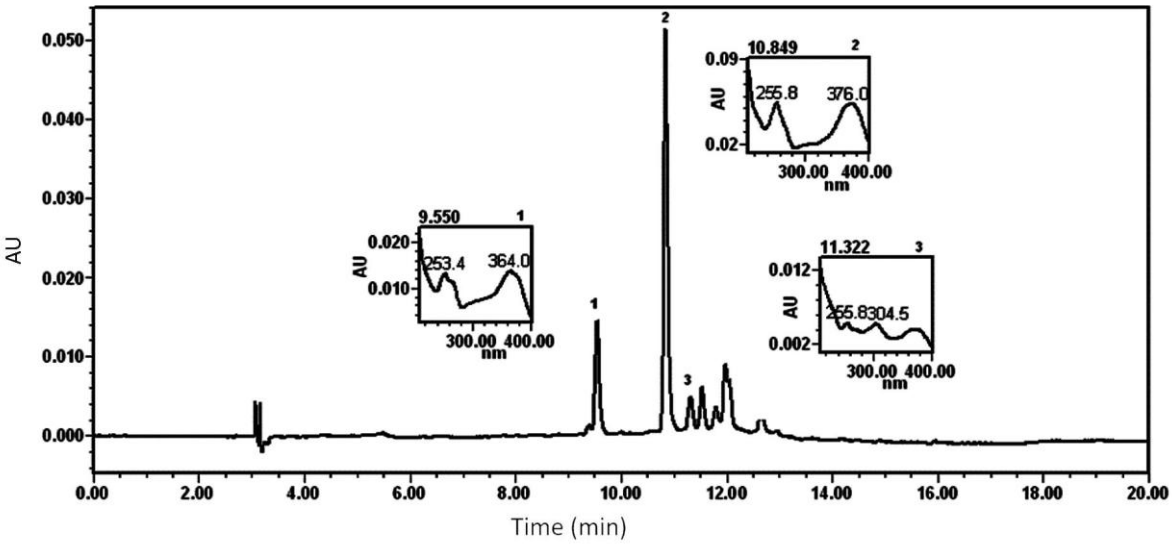

Figure 8: Chromatogram of the red onion peel extract (λ = 370 nm). (1: Quercetin glycoside, 2: Quercetin, 3: Kaempferol).

Figure 8 presents the chromatograms of QUE and its derivatives, which absorb at 370 nm, alongside other phenolic compounds absorbing at 280 nm in red onion peel extract. QUE recovery calculations were based on measurements at 370 nm. Following a 2-hour incubation of the extract with QUE-MMIP in a water bath, some non-target compounds were also retained (Figure 8). Given their phenolic structures and –OH groups, these compounds likely interacted with the polymer through hydrogen bonding or non-specific interactions within its heterogeneous regions. To eliminate retained QUE and other substances, a six-step washing procedure was implemented after QUE-MMIP treatment (Figures 8,9). Finally, to recover the QUE retained in the polymer, a two-step washing procedure was applied using 8 mL of a MeOH (8:2, v/v) mixture (Figure 9). As a result of the calculations made from the chromatograms shown in Figure 9, it was determined that 33% of QUE was recovered during the elution steps. During the washing process, quercetin glycosides and other components were removed from the medium. Table 6 shows the amounts of QUE at each stage of the process for the red onion peel extract treated with QUE-MMIP.

Table 6: QUE amounts at each processing stage of the red onion peel extract treated with QUE-MMIP.

Steps	Amount of QUE (mmol)
Loaded	2.68×10^{-5}
Adsorbed	1.68×10^{-5}
Elution 1 + Elution 2	$2.78 \times 10^{-6} + 2.72 \times 10^{-6}$
Recovery %	33 %

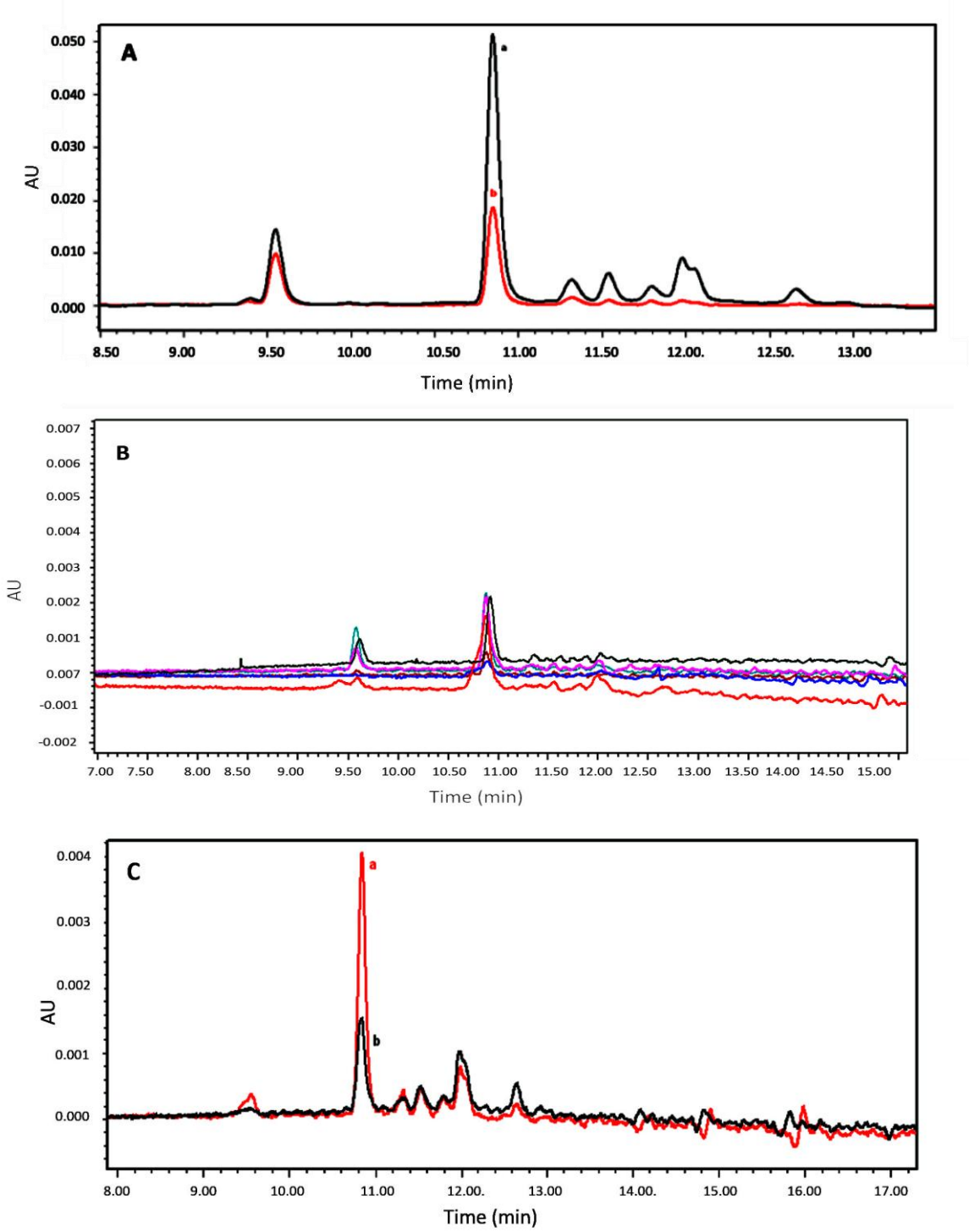

Figure 9: (A) Chromatograms of the red onion peel extract before (a) and after (b) loading (λ = 370 nm), (B)Washing chromatograms of QUE-MMIP loaded with red onion peel extract (Washing 1: 4mL H_2O, Washing 2,3,4: 4 mL 50% (v/v) EtOH), Washing 5,6: EtOH), (C) Chromatograms of the MeOH (8:2, v/v) elution following the washing steps of QUE-MMIP (λ = 370 nm). (a: elution 1, b: elution 2).

4. CONCLUSION

The synthesis of MMIPs for quercetin (QUE) is an emerging field with limited research in our country. Based on global literature, this study investigates the synthesis of QUE-imprinted polymers with magnetic properties, utilizing available resources and optimizing conditions for the best outcomes.

The targeted separation of QUE from natural matrices remains a scientific challenge, mainly due to interference from similar compounds and the limitations of traditional extraction methods. Our results show that the developed MMIP system not only overcomes these issues with improved selectivity and adsorption capacity but also allows easy magnetic separation, removing the need for filtration or centrifugation.

For the magnetic component, the method of Cai et al. (21) was adapted, with key parameters optimized, particularly the mixing speed during TEOS addition to Fe_3O_4, which was set at 800 rpm to achieve a homogeneous SiO_2 coating. Surface

modification of Fe_3O_4 was further achieved using γ-MPS to facilitate QUE binding, followed by washing to a pH range of 6.5–7.5.

QUE, a bioactive flavonoid with antioxidant, anticancer, and anti-inflammatory properties, was selected as the template molecule. Various polymerization methods (suspension, bulk, and ultrasonic) were tested, with bulk polymerization chosen for its ability to produce homogeneous polymers. Optimization studies identified 4-VP as the functional monomer, THF as the solvent, and a molar ratio of QUE: 4-VP: EDMA (1:8:40) as optimal for QUE-MMIP synthesis. AIBN was used as the initiator (20 mg). A non-imprinted polymer (MNIP) was also synthesized for comparison.

Batch adsorption tests were performed to examine how time, solvent, and concentration affect QUE uptake. The best adsorption solvent, based on the imprinting factor (BF), was 50% (v/v) ethanol, which had a BF of 1.65. The ideal rebinding time was 2 hours, after which the amount of QUE retained by both MMIP and MNIP remained steady. The highest BF values were seen at a QUE concentration of 60 µM. Static and theoretical adsorption capacities were determined, with QUE-MMIP showing a static capacity of 1496 µg/g. Freundlich and Langmuir adsorption isotherms were applied to the data, with Langmuir fitting better (R^2 > Freundlich), indicating monolayer adsorption on a uniform surface. The theoretical maximum adsorption (Qmax) for QUE-MMIP was 796 µg/g.

FTIR-ATR spectra confirmed the successful synthesis of magnetic components (SiO_2@Fe_3O_4 and γ-MPS-SiO_2@Fe_3O_4). No major differences were seen between the IR spectra of QUE-MMIP and MNIP, except for a lower peak intensity in MMIP, indicating the presence of the template molecule.

Finally, QUE-MMIP was tested for its ability to recover QUE from red onion peel extract. HPLC analysis showed that QUE was selectively adsorbed, with a recovery yield of 33%. These results, when compared to synthetic mixtures, confirmed the potential of QUE-MMIP for selective recovery of QUE from natural sources. Efficient isolation and enrichment of this bioactive flavonoid from complex matrices can facilitate its use in nutraceuticals, pharmaceuticals, and functional foods, ultimately contributing to public health by enhancing access to natural compounds with preventive and therapeutic potential.

5. CONFLICT OF INTEREST

No potential conflict of interest was reported by the author(s).

6. REFERENCES

1. Mihaylova D, Schalow S. Antioxidant and stabilization activity of a quercetin-containing flavonoid extract obtained from Bulgarian *Sophora japonica* L. Brazilian Arch Biol Technol [Internet]. 2013 Jun;56(3):431–8. Available from: <URL>.

2. Qi W, Qi W, Xiong D, Long M. Quercetin: Its antioxidant mechanism, antibacterial properties and potential application in prevention and control of toxipathy. Molecules [Internet]. 2022 Oct 3;27(19):6545. Available from: <URL>.

3. Jan AT, Kamli MR, Murtaza I, Singh JB, Ali A, Haq QMR. Dietary flavonoid quercetin and associated health benefits—An overview. Food Rev Int [Internet]. 2010 Jun 9;26(3):302–17. Available from: <URL>.

4. Shabir I, Kumar Pandey V, Shams R, Dar AH, Dash KK, Khan SA, et al. Promising bioactive properties of quercetin for potential food applications and health benefits: A review. Front Nutr [Internet]. 2022 Nov 30;9. Available from: <URL>.

5. Chen L, Li B. Application of magnetic molecularly imprinted polymers in analytical chemistry. Anal Methods [Internet]. 2012;4(9):2613. Available from: <URL>.

6. Ansari S. Application of magnetic molecularly imprinted polymer as a versatile and highly selective tool in food and environmental analysis: Recent developments and trends. TrAC Trends Anal Chem [Internet]. 2017 May;90:89–106. Available from: <URL>.

7. Ariani MD, Zuhrotun A, Manesiotis P, Hasanah AN. Magnetic molecularly imprinted polymers: An update on their use in the separation of active compounds from natural products. Polymers [Internet]. 2022 Mar 29;14(7):1389. Available from: <URL>.

8. Karimi Baker Z, Sardari S. Molecularly Imprinted Polymer (MIP) Applications in Natural Product Studies Based on Medicinal Plant and Secondary Metabolite Analysis. Iran Biomed J [Internet]. 2021 Mar 1;25(2):68–77. Available from: <URL>.

9. Malik MI, Shaikh H, Mustafa G, Bhanger MI. Recent applications of molecularly imprinted polymers in analytical chemistry. Sep Purif Rev [Internet]. 2019 Jul 3;48(3):179–219. Available from: <URL>.

10. Basak S, Venkatram R, Singhal RS. Recent advances in the application of molecularly imprinted polymers (MIPs) in food analysis. Food Control [Internet]. 2022 Sep;139:109074. Available from: <URL>.

11. Karaman Ersoy Ş, Tütem E, Sözgen Başkan K, Apak R, Nergiz C. Preparation, characterization and usage of molecularly imprinted polymer for the isolation of quercetin from hydrolyzed nettle extract. J Chromatogr B [Internet]. 2016 Apr;1017–1018:89–100. Available from: <URL>.

12. Rahimi M, Bahar S, Heydari R, Amininasab SM. Determination of quercetin using a molecularly imprinted polymer as solid-phase microextraction sorbent and high-performance liquid chromatography. Microchem J [Internet]. 2019 Jul;148:433–41. Available from: <URL>.

13. Hassan SSM, Abdel Shafy HI, Mansour MSM, Sayour HE. Quercetin recovery from onion solid

waste via solid-phase extraction using molecularly imprinted polymer nanoparticles. Int J Food Eng [Internet]. 2019 Feb 25;15(1–2). Available from: <URL>.

14. Ersoy ŞK, Tütem E, Başkan KS, Apak R. Valorization of red onion peels for quercetin recovery using quercetin-imprinted polymer. J Chromatogr Sci [Internet]. 2020 Jan 23;58(2):163–70. Available from: <URL>.

15. Abdullah, Alveroglu E, Balouch A, Khan S, Mahar AM, Jagirani MS, et al. Evaluation of the performance of a selective magnetite molecularly imprinted polymer for extraction of quercetin from onion samples. Microchem J [Internet]. 2021 Mar;162:105849. Available from: <URL>.

16. Karrat A, Palacios-Santander JM, Amine A, Cubillana-Aguilera L. A novel magnetic molecularly imprinted polymer for selective extraction and determination of quercetin in plant samples. Anal Chim Acta [Internet]. 2022 Apr;1203:339709. Available from: <URL>.

17. Huang S, Xu J, Zheng J, Zhu F, Xie L, Ouyang G. Synthesis and application of magnetic molecularly imprinted polymers in sample preparation. Anal Bioanal Chem [Internet]. 2018 Jul 12;410(17):3991–4014. Available from: <URL>.

18. Xie X, Wei F, Chen L, Wang S. Preparation of molecularly imprinted polymers based on magnetic nanoparticles for the selective extraction of protocatechuic acid from plant extracts. J Sep Sci [Internet]. 2015 Mar 2;38(6):1046–52. Available from: <URL>.

19. Cheng Y, Nie J, Li J, Liu H, Yan Z, Kuang L. Synthesis and characterization of core–shell magnetic molecularly imprinted polymers for selective recognition and determination of quercetin in apple samples. Food Chem [Internet]. 2019 Jul;287:100–6. Available from: <URL>.

20. Franqui LS, Santos MG, Virtuoso LS, Maia PP, Figueiredo EC. Synthesis and characterization of a magnetic molecularly imprinted polymer for the selective extraction of nicotine and cotinine from urine samples followed by GC-MS analysis. Anal Methods [Internet]. 2015;7(21):9237–44. Available from: <URL>.

21. Cai P shan, Zhao Y, Yang T hua, Chen J, Xiong C mei, Ruan J lan. Preparation of magnetic molecularly imprinted polymers for selective isolation and determination of kaempferol and protoapigenone in *Macrothelypteris torresiana*. J Huazhong Univ Sci Technol [Medical Sci [Internet]. 2014 Dec 6;34(6):845–55. Available from: <URL>.

22. Chiou MS, Li HY. Equilibrium and kinetic modeling of adsorption of reactive dye on cross-linked chitosan beads. J Hazard Mater [Internet]. 2002 Jul;93(2):233–48. Available from: <URL>.

23. Ng JCY, Cheung WH, McKay G. Equilibrium studies for the sorption of lead from effluents using chitosan. Chemosphere [Internet]. 2003 Aug;52(6):1021–30. Available from: <URL>.

24. Hong Y, Chen L. Extraction of quercetin from Herba Lysimachiae by molecularly imprinted-matrix solid phase dispersion. J Chromatogr B [Internet]. 2013 Dec;941:38–44. Available from: <URL>.

25. Zeng H, Wang Y, Nie C, Kong J, Liu X. Preparation of magnetic molecularly imprinted polymers for separating rutin from Chinese medicinal plants. Analyst [Internet]. 2012;137(10):2503. Available from: <URL>.

26. Sakakibara H, Honda Y, Nakagawa S, Ashida H, Kanazawa K. Simultaneous determination of all polyphenols in vegetables, fruits, and teas. J Agric Food Chem [Internet]. 2003 Jan 1;51(3):571–81. Available from: <URL>.

JOTCS A
Journal of the Turkish Chemical Society
Section: A
Chemistry

TURKISH CHEMICAL SOCIETY

Valorization of Raw Clay from Goulmima, Morocco, as A Low-Cost Mineral Adsorbent for Efficient Cationic Dye Removal

Mohammed Chrachmy[1*], Rajae Ghibate[2], Meryem Kerrou[2], Youness Achour[3], Najia Elhamzaoui[4], Ayoub Tahiri[5], Mohamed Ech-Chykry[1], Hassan Ouallal[1], Mohamed Azrour[1]

[1]Laboratory of Materials Engineering for the Environment and Natural Resources, Faculty of Sciences and Technologies, Moulay Ismail University of Meknes, Errachidia, 52000, Morocco.
[2]Laboratory of Physical Chemistry, Materials and Environment, Faculty of Sciences and Technologies, Moulay Ismail University of Meknes, Errachidia, 52000, Morocco.
[3]Laboratory of Molecular Chemistry, Materials and catalysis, Faculty of Sciences and Technologies, Sultan Moulay Slimane University, Beni-Mellal, 23000, Morocco.
[4]Higher Institute of Nursing and Health Professions of Fez-Meknes. Regional Directorate of Health Fes-Meknes, Meknes, 11201, Morocco.
[5]Laboratory of Materials, Membranes, and Nanotechnology, Faculty of Sciences, Moulay Ismail University of Meknes, Meknes, 11201, Morocco.

Abstract: Malachite green (MG), a synthetic dye extensively used in various industries, is a persistent and toxic pollutant that poses serious risks to aquatic ecosystems and human health. The limitations of conventional dye removal methods highlight the need for efficient and sustainable alternatives. In this context, the present study investigates the potential of raw Goulmima clay from Morocco as a low-cost adsorbent for the removal of MG from aqueous solutions. Experiments were carried out to examine the impact of different factors on the adsorption process, including thermodynamic, kinetic, and adsorption isotherm analyses. The findings indicate that the mass of adsorbent, initial solute concentration, stirring speed, temperature, and contact time affect how well malachite green adsorbs onto the clay. Increasing adsorbent of mass from 10 to 50 mg leads to a decrease in the adsorbed quantity from 60 to 13 mg/g. Conversely, raising the initial malachite green concentration from 5×10^{-6} to 10^{-4} M increased the quantity adsorbed from 2.60 to 39.86 mg/g within five minutes. Adsorption equilibrium was reached within 40 minutes. Both temperature and stirring speed had a slight positive effect, indicating the endothermicity of the process, as supported by the thermodynamic results. The isothermal and kinetic model evaluations indicated a strong fit between the experimental data and the non-linear forms of the Langmuir model and the pseudo-second-order model. Comparative analysis with other mineral materials shows that raw Goulmima clay demonstrates superior adsorption efficiency for malachite green. This positions it as a more effective and cost-efficient adsorbent than many other commonly used mineral materials. These findings suggest that the studied clay holds significant promise for practical applications in cleaning water loaded with malachite green dye.

Keywords: Malachite green, Raw clay, Adsorption, Parametric effects, Kinetic study, Isotherm study.

Submitted: October 8, 2024. **Accepted:** June 30, 2025.

Cite this: Chrachmy M, Ghibate R, Kerrou M, Achour Y, Elhamzaoui N, Tahiri A, Ech-Chykry M, Ouallal H, Azrour M. Valorization of Raw Clay from Goulmima, Morocco, as A Low-Cost Mineral Adsorbent for Efficient Cationic Dye Removal. JOTCSA. 2025;12(3): 169-80.

DOI: https://doi.org/10.18596/jotcsa.1562444

***Corresponding author's E-mail:** mo.chrachmy@edu.umi.ac.ma

1. INTRODUCTION

Synthetic dyes play a crucial role in various industries due to their desirable properties, such as consistent coloration, high color fastness, excellent efficiency, and low production cost (1). They are extensively used in sectors such as textiles, leather, paper, plastics, cosmetics, printing, paints, and food, fulfilling both aesthetic and functional roles (2). However, the extensive use of these dyes has

led to significant environmental concerns (3–5). Among these dyes, cationic ones are of particular concern because of their persistence in aquatic environments, making them significant water pollutants (6). A notable example is malachite green (MG), a synthetic cationic dye belonging to the triphenylmethane class. MG is widely used for dyeing silk, wool, leather, and paper, owing to its intense color and strong affinity for various substrates (7,8). It is also employed in aquaculture due to its antifungal and antiparasitic properties (9,10). However, its use has been banned or restricted in many countries because of growing concerns about its toxicity, carcinogenic potential, and environmental persistence (11). MG is notably resistant to removal from aqueous solutions (12), leading to significant detrimental consequences for aquatic life and human health (13). In aquatic ecosystems, MG exhibits acute and chronic toxicity to a wide range of organisms, including algae, crustaceans, and fish (14–16). The dye can bioaccumulate in aquatic organisms, leading to histopathological changes, reproductive dysfunction, and genotoxicity (17). Moreover, the bioaccumulated dye can be transferred through the food chain, posing a risk to predators and even humans who consume contaminated aquatic species (18). The toxicological profile of MG in humans is also concerning. MG is classified as a Class II health hazard due to its harmful effects on human health (19). Studies have shown that exposure to MG can cause various health issues, including gastrointestinal irritation, increased heart rate, jaundice, and ocular damage (20–22). More importantly, MG and its primary metabolite, leucomalachite green, have been shown to exhibit mutagenic, carcinogenic, teratogenic, and cytotoxic effects in mammalian cells (14,23). As a result, several countries have introduced regulatory measures, including bans on its use (24). Nonetheless, its continued use in unregulated sectors contributes to its persistent presence in the environment. Given these environmental and health hazards, numerous efforts have been directed toward the removal or degradation of MG from wastewater before it enters natural water bodies (25). Various technological approaches have been considered to address the removal of MG, including solar irradiation (26), sonochemical degradation (27), advanced oxidation processes, membrane technology (28), and biological treatments (29,30). Each method has its own limitations in terms of cost, design and removal efficiency. Overall, the effectiveness and cost-effectiveness of these processes are not entirely clear-cut (31). Adsorption, in contrast, has emerged as a simple, cost-effective, and efficient approach for removing dyes and other organic pollutants from wastewater (32,33). This technique offers advantages such as flexibility in design, low energy requirements, fast kinetics, and the possibility of regeneration and reuse of the adsorbent material. The key to a successful adsorption process lies in the choice of adsorbent, which should be efficient, economical, readily available, and environmentally benign. In this context, natural clays have gained significant attention as promising adsorbents for environmental remediation (34). Owing to their abundance, low cost, non-toxicity, sustainability, and remarkable adsorption capacities, clays stand out as excellent candidates for wastewater treatment applications (35–39). Due to their porous structure, clays provide a highly specific surface area that enhances their ability to capture molecules efficiently. The variety of pore sizes in clays facilitates the adsorption of substances based on their size and polarity. Additionally, the surface electric charge of clays attracts and retains charged ions and molecules. The ordered crystalline structure and the chemical composition of clays, including the presence of exchangeable ions, further contribute to their adsorption efficiency. Moreover, the sheet-like arrangement of minerals in clays creates interfoliar spaces that are conducive to adsorption. These characteristics make clays the preferred choice for water purification through adsorption. The present study investigates the adsorption potential of raw Goulmima clay, a natural mineral sourced from southeastern Morocco, for malachite green removal from aqueous media. Despite its regional abundance, this clay remains underexplored in environmental remediation. The study evaluates the influence of key operational parameters, including adsorbent dosage, initial dye concentration, contact time, temperature, and stirring speed, on the adsorption performance. To gain insight into the adsorption mechanism and behavior, well-established kinetic models (Pseudo-First-Order, Pseudo-Second-Order, and Intra-Particle Diffusion) and equilibrium isotherm models (Langmuir and Freundlich) were applied. These models were selected based on their wide use and reliability in previous studies involving dye removal using natural and mineral-based adsorbents (40–42). Furthermore, thermodynamic analyses were conducted to assess the spontaneity and nature of the adsorption process.

2. EXPERIMENTAL

2.1. Adsorbent

The clay selected for this study was sampled from Goulmima City, Morocco. After sampling, the clay underwent crushing, grinding, and sieving using sieves conforming to ISO standards. The fraction less than 315 µm was retained for the adsorption experiments. The resulting powder of raw Goulmima clay is referred to as RCG in this study.

2.2. Adsorbate

The dye used in this investigation is malachite green oxalate, supplied by VWR, with the chemical formula $C_{52}H_{54}N_4O_{12}$. Figure 1 illustrates the dye molecule's chemical structure. A series of well-defined concentrations was prepared by diluting a stock solution, which was created by dissolving the accurately measured color powder in deionized water.

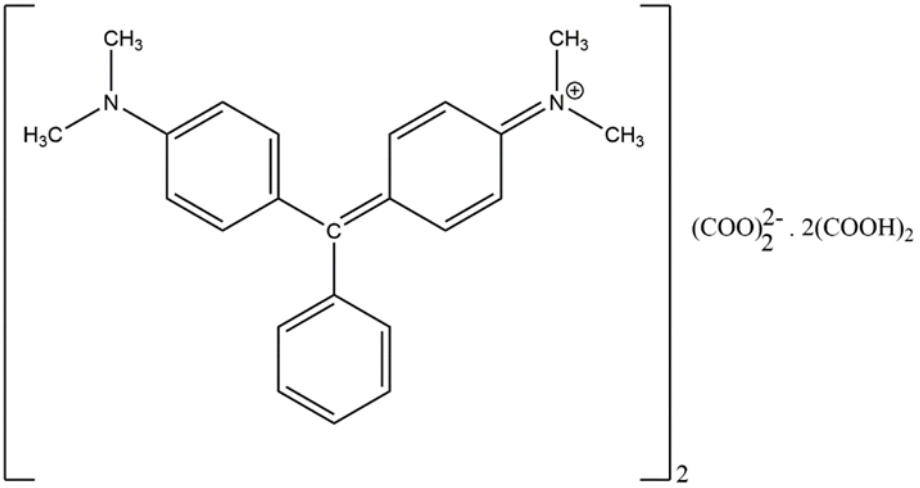

Figure 1: Chemical structure of malachite green oxalate.

2.3. Batch Adsorption Experiments

The primary objective of this section is to analyze and optimize the key parameters influencing the adsorption of MG onto RCG. These parameters include time of contact, adsorbent mass, temperature, agitation speed, and initial MG concentration. The effect of each parameter was evaluated over an adsorption time ranging from five to sixty minutes. To evaluate the impact of adsorbent mass, three different masses (0.10, 0.25, and 0.50 g) were introduced into 150 mL of MG solution at a concentration of 5×10^{-5} M. Experiments were conducted at room temperature with stirring at 250 rpm. A mass of 0.25 g was then selected for other parameter studies. The effect of agitation speed was investigated across a range from 250 to 750 rpm at 25 °C, using a 5×10^{-5} M MG concentration solution. The effect of initial concentration of dye was evaluated over a range of 5×10^{-6} to 10^{-4} M at an agitation speed of 250 rpm at 25 °C.

Additionally, the influence of temperature was evaluated by conducting adsorption tests at 25, 35, and 45°C while stirring at 250 rpm with a dye concentration of 5×10^{-5} M. These conditions were also used for the thermodynamic study. In the isotherm study, several experiments were performed for 90 minutes at 25 °C, across a concentration range of 5 to 150 mg/L, under optimal conditions: a clay mass of 0.25 g, a stirring rate of 250 rpm, and the natural pH of the medium.

Following each test, the mixture was separated by filtration, and the MG residual concentration was determined using a UV/visible spectrometer (UV-160, Shimadzu) at the maximum absorption wavelength of 620 nm. Subsequently, the equation as below was employed to calculate the adsorbed quantity:

$$q_t = \frac{M_{MG}(C_0 - C_t)}{m} \times V_{MG} \quad (1)$$

Where:

q_t : Amount of dye adsorbed at time t (mg/g)
C_0 : Initial concentration (M)
C_e : Residual concentration at time t (M)
V_{MG} : Volume of the malachite green solution (L)
M_{MG} : Molar mass of malachite green (g/mol)
m : Mass of clay (g)

2.4. Thermodynamic Study

Adsorption thermodynamics parameters (standard enthalpy change (ΔH°), standard entropy change (ΔS°), and standard free energy change (ΔG°)) were investigated to provide insights into the nature and spontaneity of adsorption reactions.

The equations below were used to obtain ΔG°:

$$\Delta G^\circ = -RT\ln K_d \quad (2)$$

$$\Delta G^\circ = \Delta H^\circ - T\Delta S^\circ \quad (3)$$

Where T is the absolute temperature (K) and R is the gas constant (8.314 J.mol^{-1}.K^{-1}).

K_d refers to the distribution constant, which can be expressed as follows:

$$K_d = \frac{C_e}{q_e} \quad (4)$$

The combination of equations (2), (3), and (4) yields the following equation:

$$\ln K_d = -\frac{\Delta G^\circ}{RT} = \frac{-\Delta H^\circ}{RT} + \frac{\Delta S^\circ}{R} \quad (5)$$

Plotting ln K_d versus 1/T yields an affine function. ΔH° and ΔS° are obtained from the slope and the intercept of this plot, respectively (13).

2.5. Kinetic Modeling

For a better understanding of the adsorption of malachite green onto RCG, three kinetic models were employed: the Pseudo-First-Order model (PFO), the Pseudo-Second-Order model (PSO), and the Intra-Particle Diffusion model (IDM). Both the linear and non-linear forms of the PFO and PSO models were utilized. The modeling was based on kinetic adsorption data collected under the following experimental conditions: 0.25 g of clay, 25 °C, an initial dye concentration of 5×10^{-5} M, and an agitation speed of 250 rpm. The equations corresponding to the linear and non-linear forms of

the PFO (Eqs. 6 and 7) and PSO (Eqs. 8 and 9) models, as well as the IDM (Eq. 10) (44,45), are provided below.

$$q_t = q_e\left(1 - e^{-k_1 t}\right) \quad (6)$$

$$\ln(q_e - q_t) = \ln q_e - k_1 t \quad (7)$$

$$q_t = \frac{q_e^2 k_2 t}{q_e k_2 t + 1} \quad (8)$$

$$\frac{t}{q_t} = \frac{1}{k_2 q_e^2} + \frac{t}{q_e} \quad (9)$$

$$q_t = k_{idp}\, t^{1/2} + c \quad (10)$$

Where:
q_e : Amount of dye adsorbed at equilibrium (mg/g)
k_1 : Rate constante of the pseudo-first-order model (min^{-1})
k_2 : Rate constante of the pseudo-second-order model ($g \cdot mg^{-1} \cdot min^{-1}$)
k_{ipd}: Rate constant associated with the intraparticle diffusion model ($mg \cdot g^{-1} \cdot min^{-1/2}$)
c: Boundary layer thickness

2.6. Equilibrium Isotherm Modeling

To gain a clearer understanding of MG adsorption onto RCG, an isotherm study was performed. The equilibrium data were fitted to both the non-linear and linear forms of the Langmuir (Eqs. 11 and 12) and Freundlich (Eqs. 13 and 14) models (46,47).

$$q_e = \frac{q_{max} K_L C_e}{1 + K_L C_e} \quad (11)$$

$$q_e = \left(\frac{1}{q_{max} K_L}\right) * \frac{1}{C_e} + \frac{1}{q_{max}} \quad (12)$$

$$q_e = K_F C_e^{1/n} \quad (13)$$

$$\ln q_e = \ln K_F + \frac{1}{n} * \ln\, C_e \quad (14)$$

Where:
C_e : Concentration of the dye remaining in solution at equilibrium (mg/L)
q_{max} : Maximum adsorption capacity (mg/g),
K_L : Langmuir constant (L/mg)
K_F : Freundlich coefficient related to the adsorption capacity $(mg/g)(L/g)^n$
n : Freundlich's affinity coefficient (-)

2.7. Error Analysis

The model adaptation was evaluated using error function analyses, including the coefficient of determination (R^2, Eq. 15), Root Mean Square Error (RMSE, Eq. 16), and chi-square (χ^2, Eq. 17) (45,48).

$$R^2 = \frac{\sum_{i=1}^{n}(q_{cal} - \overline{q_{exp}})^2}{\sum_{i=1}^{n}(q_{cal} - \overline{q_{exp}})^2 + \sum_{i=1}^{n}(q_{cal} - q_{exp})^2} \quad (15)$$

$$RMSE = \sqrt{\frac{1}{n} \times \sum_{i=1}^{n}(q_{exp,i} - q_{cal,i})^2} \quad (16)$$

$$\chi^2 = \sum_{i=1}^{n} \frac{(q_{exp} - q_{cal})^2}{q_{cal}} \quad (17)$$

3. RESULTS AND DISCUSSION

3.1. Characterization of Clay Particles

The RCG material used in this study, previously characterized in our earlier work, is primarily composed of 34.1% silica, 10.5% alumina, and 22.1% calcium, as indicated by X-ray fluorescence analysis. X-ray diffraction reveals that RCG is mainly composed of quartz, kaolinite, and illite. Thermogravimetric analysis demonstrates high thermal stability of RCG up to 800 °C, with a minimal mass loss due to adsorbed surface water. The derivative thermogravimetric analysis reveals two endothermic peaks: the first at 120 °C, corresponding to dehydration, and the second at 656 °C, corresponding to dehydroxylation, which leads to the formation of metakaolinite. The BET method indicates a type IV isotherm, characteristic of mesoporous materials, with an H_3 hysteresis indicating non-uniform pores. The key parameters obtained by the BET method are an average pore diameter around 38.36 Å, and a specific surface area of 25.35 m^2/g. The pHpzc of RCG, crucial for adsorption, is approximately 7.84, providing an understanding of the adsorbent surface charge characteristics (49).

3.2. Adsorption Study

Adsorption occurs when MG binds to the surface of RCG. This process is influenced not only by the characteristics of the clay and the dye molecule but also by operational batch parameters. Understanding how these factors affect the system under study is essential. Figure 2 illustrates four parameter effects on MG adsorption onto RCG over time. According to the data, under all experimental conditions, the amount of MG adsorbed increases rapidly during the first five minutes, after which the rate of adsorption slows down. This initial sharp rise is attributed to the availability of active sites, which progressively become saturated as the adsorption process continues (42). Figure 2(a) shows that as the adsorbent mass increases, the adsorbed amount of dye decreases. This trend suggests that at lower clay masses, the particles disperse more effectively in the solution, enhancing the accessibility of active sites and facilitating the adsorption of dye molecules onto the clay surface. The decrease is primarily due to adsorbent aggregation and site competition (50). Figure 2(b) shows the effect of initial dye concentration on MG adsorption. As the initial concentration increases from 5×10^{-6} M to 1×10^{-4} M, the adsorbed amount also increases from 2.703 mg/g to 45.037mg/g. This behavior is attributed to the increase in the concentration gradient, which serves as the driving force for mass transfer, enhancing the diffusion of dye molecules from the bulk solution to the surface of RCG. However, this enhancement has a limit. Once the active adsorption sites on the clay surface become saturated, further increases in the initial concentration do not result in significant additional adsorption, as the system approaches equilibrium (51). Figure 2(c) shows the effect of temperature on MG adsorption onto RCG. The amount adsorbed increases slightly, from 26.85 mg/g at 25 °C to 27.45 mg/g at 45 °C. This trend suggests an endothermic process (52). Higher temperatures enhance the mobility of dye molecules. They also improve diffusion through the external boundary layer. As a result, more active sites on the clay surface become accessible. The endothermic nature of the process is further supported by the positive enthalpy change ($\Delta H° = 39.98\ kJ \cdot mol^{-1}$) of the

system. In addition, the activation energy (Ea), estimated using the Arrhenius equation between 25 °C and 45 °C, was found to be 13.85 kJ·mol⁻¹. This relatively low Ea confirms that the energy barrier for adsorption is moderate and can be easily overcome by increasing the temperature, thus promoting the diffusion of MG molecules toward available adsorption sites on the clay surface. Figure 2(d) illustrates the effect of agitation speed on MG adsorption. The results indicate that as the agitation speed increases, the amount of MG adsorbed also rises slightly, reaching a value of 27.66 mg/g at 750 rpm. This enhancement is attributed to improved mass transfer conditions. Specifically, higher agitation speeds reduce the thickness of the external boundary layer surrounding the adsorbent particles. This allows dye molecules to diffuse more easily to the active sites on RCG. As a result, MG adsorption becomes more efficient (22).

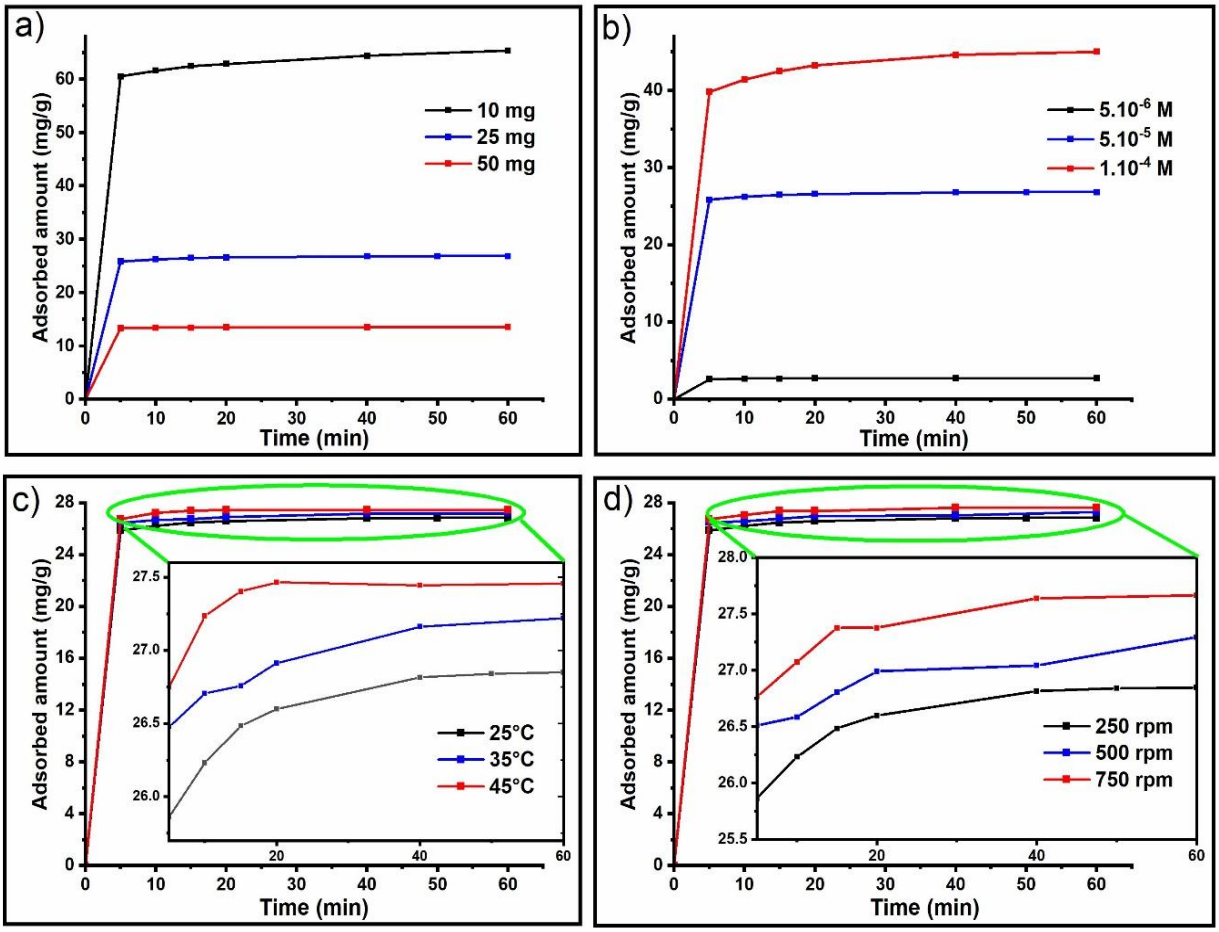

Figure 2: Effect of Parameters on the Adsorption of MG onto RCG.

3.3. Thermodynamic Study

A study of the variation of $\ln K_d$ with the inverse of temperature reveals a straight line, where the slope corresponds to ΔH° and the y-intercept represents ΔS°. The values obtained are presented in Table 1, along with the calculated ΔG° values. The findings reveal that the adsorption of MG on the studied clay occurs spontaneously, as evidenced by the negative values of ΔG°, and the spontaneity increases with the temperature (53). The positive ΔH° value confirms that the process is endothermic. Additionally, the positive ΔS° value suggests that the adsorption induces an increase in disorder at the interface between MG and RCG (54).

Table 1: Thermodynamic parameters for MG adsorption onto RCG.

Adsorbent	Temperature (K)	ΔG° (KJ.mol^{-1})	ΔH° (KJ. mol^{-1})	ΔS° (J.mol^{-1}. K^{-1})
RCG	298	-41.047	39.980	271.693
	308	-43.705		
	318	-46.493		

3.4. Kinetic Study

Figure 3 illustrates the modeling of adsorption kinetics of MG onto RCG clay using both the non-linear and linear forms of the PFO and PSO. Table 2 displays the kinetic parameters along with associated statistical error values. The results indicate that among the kinetic models evaluated, the non-linear PSO model provided the best fit to the experimental data, as evidenced by the lowest RMSE and χ^2 values, confirming its suitability for describing the adsorption process. In contrast, the linear form of the pseudo-first-order model exhibited a poor fit. The calculated equilibrium adsorption capacity ($q_{e,cal}$= 1.747 mg/g) was significantly lower than the experimental value ($q_{e,exp}$= 26.85 mg/g), indicating that the model fails to represent the actual adsorption behavior. Furthermore, the PFO linear form showed an extremely high χ^2 value (3069.176), in stark contrast to the values near zero observed for the other models. This substantial deviation confirms that the linear PFO model is not appropriate for describing the adsorption kinetics of the studied system. Based on these findings, it can be concluded that the studied system follows pseudo-second-order kinetics.

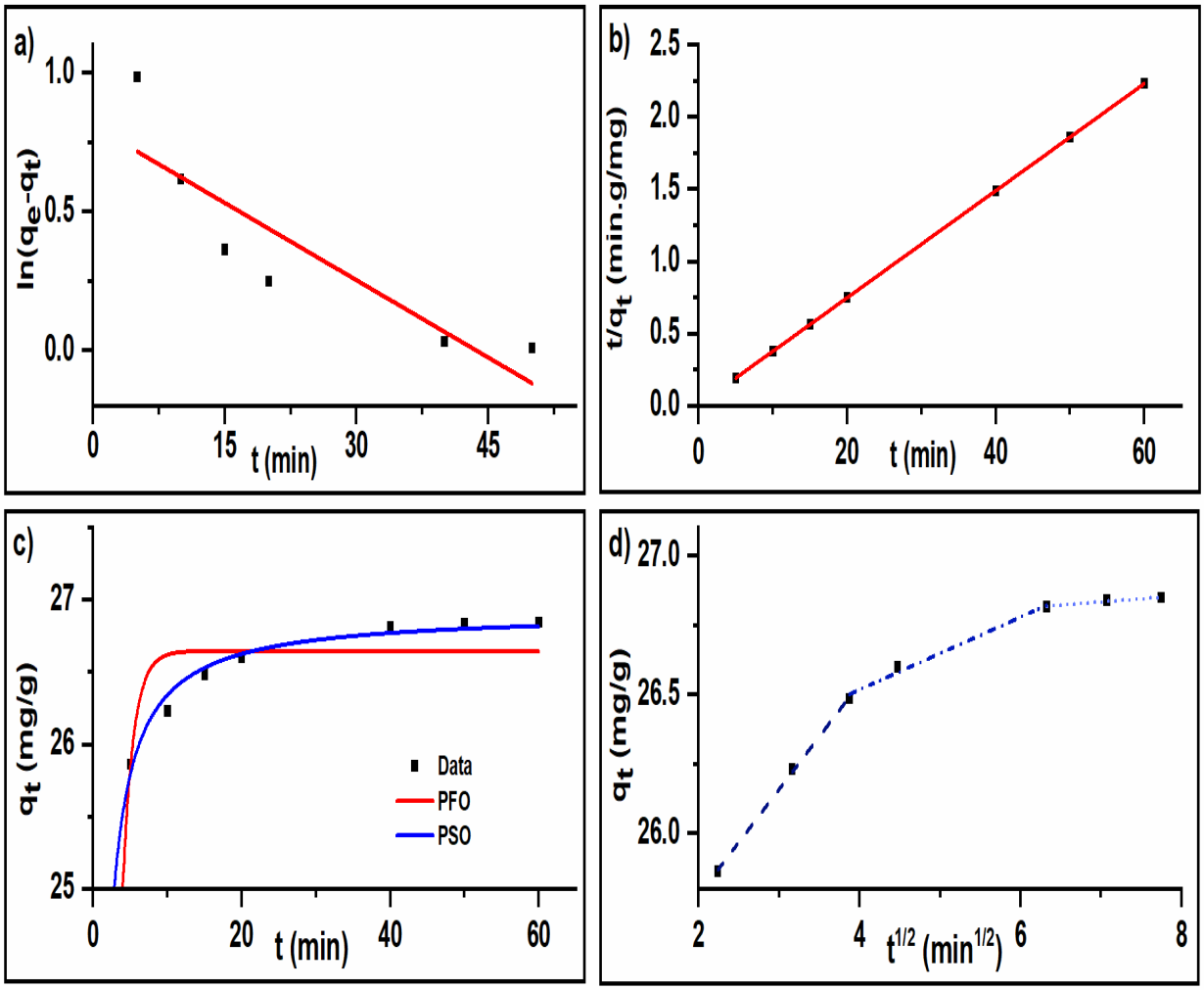

Figure 3: Graphical representations of the linear forms of PFO (a) and PSO (b), the non-linear forms of PFO and PSO (c), and the intra-particle diffusion model (d).

Table 2: Parameters and statistical errors associated with kinetic modeling.

Parameter & statistical error	Adsorption kinetic model			
	PFO		PSO	
	LF	NLF	LF	NLF
$q_{e,\ cal}$ (mg/g)	1.747	26.646	26.969	26.917
Relative error (%)	93.492	0.75	0.443	0.249
$k_1(min^{-1})$ /k_2 $(g.mg^{-1}.min^{-1})$	0.103	0.700	0.145	0.171
R^2	0.9971	0.9995	1.0000	0.9999
X^2	3069.176	0.011	0.002	0.001
RMSE	23.729	0.190	0.079	0.0553

Figure 3 (d) shows multi-linear intra-particle diffusion plots that do not pass through the origin. This demonstrates that intra-particle diffusion is not the rate-limiting step controlling the adsorption of MG on RCG. External mass transfer is indicated by the initial linear section with a steep slope, while intra-particle diffusion is illustrated by the second section, and equilibrium is signified by the plateau region (55).

Table 3: Kinetic parameters from the intra-particle diffusion model.

Step	Parameter	Value
First step	$k_{idp,1}$ (mg/g.min$^{1/2}$)	0.062
	C_1	25.571
	R^2_1	0.9883
Second step	$k_{idp,2}$ (mg/g.min$^{1/2}$)	0.013
	C_2	26.321
	R^2_2	0.9747
Third step	$k_{idp,3}$ (mg/g.min$^{1/2}$)	0.002
	C_3	26.753
	R^2_3	0.9382

3.5. Isotherm Study

Figure 4 presents the experimental data from the isotherm study alongside the predictions generated by both the linear and non-linear forms of the Freundlich and Langmuir isothermal models. The results are summarized in Table 4. Although the linear Langmuir model shows a slightly higher correlation coefficient (R^2= 0.9965) than the nonlinear form (R^2= 0.9915), the latter provides a better overall fit, as indicated by lower error values (RMSE=1.3578; χ^2= 1.733). These results suggest that MG adsorption occurs as a monolayer on energetically uniform sites, with minimal interaction between adsorbed molecules, which is consistent with the assumptions of the Langmuir model (56), which is in accordance with the fundamental assumptions of the Langmuir model. Concerning the Freundlich model R^2 values (0.811 (LF) and 0.8456 (NLF)) are significantly lower than Langmuir. Concerning the Freundlich model, R^2 values (0.811 (LF) and 0.8456 (NLF)) are significantly lower than Langmuir. The model in both forms shows higher error values (Table 4), which further confirms its inadequacy in describing the adsorption process under study.

In terms of adsorption capacity, the nonlinear Langmuir model predicts a maximum adsorption capacity (q_{max} = 47.703 mg/g) that is very close to the experimental value (q_{max}, exp = 46.369 mg/g), with a relative error of only 2.88%. In contrast, the linear form slightly overestimates this capacity (q_{max}= 50.075 mg/g), with a relative error of 7.99%. For the Freundlich isotherm, the estimated maximum adsorption capacity deviates more significantly from the experimental value, with relative errors of 13.36% (LF) and 42.63% (NLF). These error values highlight the limited predictive capability of the Freundlich model for the studied system.

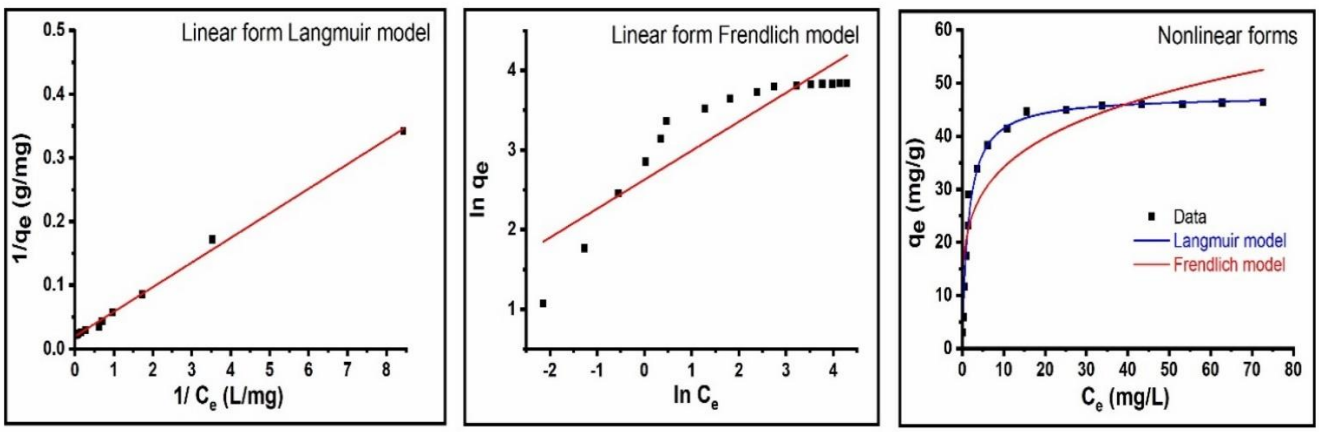

Figure 4: Fitting of the adsorption isotherm of MG at 25°C using the Freundlich and Langmuir models.

Table 4: Freundlich and Langmuir isothermal constants with error analysis.

q_{max}, exp (mg/g) = 46.369					
Langmuir			**Freundlich**		
Parameter	**LF**	**NLF**	**Parameter**	**LF**	**NLF**
$q_{max, cal}$ (mg/g)	50.075	47.703	$q_{max, cal}$ (mg/g)	66.137	52.565
Relative error (%)	7.992	2.877	Relative error (%)	42.632	13.362
K_L (L/mg)	0.001	0.668	K_F (mg/g)	13.878	20.728
R_L	0.996-0.896	0.230-0.010	1/n	0.364	0.217
R^2	0.9965	0.9915	R^2	0.811	0.8456
χ^2	2.622	1.733	χ^2	45.876	26.354
RMSE	2.0694	1.3578	RMSE	9.5585	5.7874

A key characteristic of the Langmuir isothermal model is the equilibrium parameter R_L, which is a dimensionless coefficient. It is calculated using the following equation:

$$R_L = \frac{1}{1+ K_L C_0} \quad (18)$$

Depending on the value of R_L, the process of adsorption can be classified as favorable ($0<R_L<1$), linear ($R_L \approx 1$), irreversible ($R_L=0$), or unfavorable ($R_L>1$) (57). For the studied system, the R_L values range from 0.230 to 0.010 for the non-linear Langmuir model and from 0.996 to 0.896 for the linear form, indicating favorable adsorption across all initial dye concentrations, regardless of the model used. The variation in R_L values between the two forms stems from the different K_L values obtained through the distinct mathematical fitting approaches applied in the linear and non-linear models.

3.6. Comparative Study

Table 5 shows that RCG exhibits significantly higher adsorption efficiency than other mineral materials, demonstrating its substantial potential for removing MG dye. This indicates that RCG is an effective and promising material for purifying MG-contaminated effluents.

Table 5: The maximum adsorption capacity q_{max} (mg/g), of MG from the literature by various adsorbents.

Adsorbent	**Q_{max} (mg/ g)**	**Reference**
Bentonite clay	7.720	(58)
Clay-chitosan	12.010	(59)
MgO impregnated clay	17.200	(60)
HCl treated kaolin	18.510	(61)
Diatomite	23.640	(62)
Clinoptilolite zeolite	43.860	(63)
4A zeolite	45.640	(64)
Calcium silicate	59.950	(65)
Raw clay of Goulmima (RCG)	46.369	This study

4. CONCLUSION

This study demonstrates that raw Goulmima clay (RCG) is a suitable and efficient adsorbent for the removal of malachite green (MG) from aqueous solutions. The adsorption process is significantly influenced by key operational parameters such as contact time, adsorbent mass, initial dye concentration, agitation speed, and temperature. The process is remarkably rapid, achieving an adsorption capacity of 39.86 mg/g within 5 minutes at an initial MG concentration of 10^{-4}M. The increased adsorption capacity with rising temperature suggests that the process is endothermic, likely due to enhanced diffusion of dye molecules through the external boundary layer and into the internal pores of the RCG particles. This observation is supported by the low activation energy value (13.85 kJ/mol). Furthermore, the negative ΔG° values and the positive ΔH° confirm the spontaneous and endothermic nature of the adsorption, while the positive ΔS° indicates increased randomness at the solid-liquid interface during the process. Beyond correlation coefficients (R^2), model accuracy was evaluated using RMSE and χ^2 error functions. Results show that the non-

linear forms of both kinetic and isotherm models best fit the experimental data. The pseudo-second-order model best describes the adsorption kinetics, indicating a surface-controlled mechanism, whereas intra-particle diffusion is not the primary rate-limiting step. The Langmuir isotherm provides the best fit to equilibrium data, with a maximum adsorption capacity of 47.703 mg/g (closely matching the experimental value of 46.369 mg/g), confirming the monolayer adsorption behavior. The dimensionless separation factor (R_L) values further indicate favorable adsorption of MG onto RCG. Comparative analysis reveals that RCG offers a cost-effective and high-performance alternative to other mineral adsorbents, positioning it as a promising material for the environmental remediation of dye-contaminated wastewater.

5. CONFLICT OF INTEREST

The authors declare that they have no conflicts of interest related to the publication of this paper.

6. ACKNOWLEDGMENTS

The authors also thank everyone who helped prepare the manuscript.

7. REFERENCES

1. Benjelloun M, Miyah Y, Ssouni S, Iaich S, El-habacha M, Lagdali S, et al. *Capparis spinosa* L waste activated carbon as an efficient adsorbent for crystal violet toxic dye removal: Modeling, optimization by experimental design, and ecological analysis. Chinese J Chem Eng [Internet]. 2024 Jul;71:283–302. Available from: <URL>.

2. Nitayaphat W, Jintakosol T. Green, eco-friendly and sustainable alternative in dyeing sugarcane leaves-cotton blended yarn using aqueous extract *Ficus lyrata* leaves dye: Effects of metal salts mordanting agents and mordanting methods. J Nat Fibers [Internet]. 2025 Dec 31;22(1). Available from: <URL>.

3. Patel D, Singh A, Ambati SR, Singh RS, Sonwani RK. An overview of recent advances in treatment of complex dye-containing wastewater and its techno-economic assessment. J Environ Manage [Internet]. 2024 Nov;370:122804. Available from: <URL>.

4. Ghibate R, Chrachmy M, Alaqarbeh M, Ansari A, Ben Baaziz M, Bouachrine M, et al. Comprehensive analysis of hazardous dye adsorption onto a green adsorbent: Experimental profiling, theoretical modeling, and deciphering potential molecular interactions. Desalin Water Treat [Internet]. 2025 Jan;321:100998. Available from: <URL>.

5. Ghibate R, Chrachmy M, Kerrou M, Ben Baaziz M, Alaqarbeh M, Amechrouq A, et al. Eco-friendly adsorption of Rhodamine B dye using *Punica granatum* peel from an aqueous medium. Green Anal Chem [Internet]. 2025 Mar;12:100201. Available from: <URL>.

6. Liu J, Zhu H, Qiang Z, Zhao Q, Que C, Liu C, et al. Adsorption of cationic organic dyes from aqueous solutions by sulfonated covalent organic frameworks: Characterization and mechanistic explanations. Sep Purif Technol [Internet]. 2025 Aug;364:132466. Available from: <URL>.

7. Lam SM, Low XZD, Wong KA, Sin JC. Sequencing coagulation–photodegradation treatment of malachite green dye and textile wastewater through ZnO micro/nanoflowers. Chem Eng Commun [Internet]. 2018 Aug 3;205(8):1143–56. Available from: <URL>.

8. Khan MR, Wabaidur SM, Busquets R, Khan MA, Siddiqui MR, Azam M. Identification of malachite green in industrial wastewater using lignocellulose biomass composite bio-sorbent and UPLC-MS/MS: A green environmental approach. Process Saf Environ Prot [Internet]. 2019 Jun;126:160–6. Available from: <URL>.

9. Kwan PP, Banerjee S, Shariff M, Ishak NAS, Yusoff FM. Quantitative analysis of malachite green and leucomalachite green residues in fish purchased from the markets in Malaysia. Food Control [Internet]. 2018 Oct;92:101–6. Available from: <URL>.

10. Yadav J, Qanungo K. A review: On malachite green; synthesis, uses and toxic effects. In 2023. p. 030020. Available from: <URL>.

11. Youssef EE, Beshay BY, Tonbol K, Makled SO. Biological activities and biosorption potential of red algae (*Corallina officinalis*) to remove toxic malachite green dye. Sci Rep [Internet]. 2023 Aug 24;13(1):13836. Available from: <URL>.

12. Elwardany RE, Shokry H, Mustafa AA, Ali AE. Influence of the prepared activated carbon on cellulose acetate for malachite green dye removal from aqueous solution. Macromol Res [Internet]. 2023 Nov 22;31(11):1043–60. Available from: <URL>.

13. Yadav J, Marwah H, Pant J, Kumar J. Optimizing malachite green dye removal with nano-silica clay in fixed-bed reactors. J Nanoparticle Res [Internet]. 2024 Sep 7;26(9):212. Available from: <URL>.

14. Gharavi-nakhjavani MS, Niazi A, Hosseini H, Aminzare M, Dizaji R, Tajdar-oranj B, et al. Malachite green and leucomalachite green in fish: A global systematic review and meta-analysis. Environ Sci Pollut Res [Internet]. 2023 Mar 15;30(17):48911–27. Available from: <URL>.

15. Sharma J, Sharma S, Soni V. Toxicity of malachite green on plants and its phytoremediation: A review. Reg Stud Mar Sci [Internet]. 2023 Sep;62:102911. Available from: <URL>.

16. Bora R, Rasid SS, Hussain MA. Toxicological impact of malachite green on freshwater fish: A comprehensive review. UTTAR PRADESH J Zool [Internet]. 2024 Aug 31;45(17):659–68. Available from: <URL>.

17. Srivastava S, Sinha R, Roy D. Toxicological

effects of malachite green. Aquat Toxicol [Internet]. 2004 Feb;66(3):319–29. Available from: <URL>.

18. Pipoyan D, Stepanyan S, Beglaryan M, Stepanyan S, Mantovani A. Health risk assessment of toxicologically relevant residues in emerging countries: A pilot study on malachite green residues in farmed freshwater fish of Armenia. Food Chem Toxicol [Internet]. 2020 Sep;143:111526. Available from: <URL>.

19. Lin Z, Wang D, Zhang H, Li L, Huang Z, Shen J, et al. Extraction and determination of malachite green from aquatic products based on molecularly imprinted polymers. Sep Sci Technol [Internet]. 2016 Jul 2;51(10):1684–9. Available from: <URL>.

20. Joseph F, Agrawal YK, Rawtani D. Behavior of malachite green with different adsorption matrices. Front Life Sci [Internet]. 2013 Dec 17;7(3–4):99–111. Available from: <URL>.

21. Velpandian T, Saha K, Ravi AK, Kumari SS, Biswas NR, Ghose S. Ocular hazards of the colors used during the festival-of-colors (Holi) in India—Malachite green toxicity. J Hazard Mater [Internet]. 2007 Jan;139(2):204–8. Available from: <URL>.

22. Yadav J, Sahu O. Malachite green dye purification from effluent using synthesized ceramic clay: Characterisation; optimization and scale up. Ceram Int [Internet]. 2023 Aug;49(15):24831–51. Available from: <URL>.

23. Fessard V, Godard T, Huet S, Mourot A, Poul JM. Mutagenicity of malachite green and leucomalachite green in *in vitro* tests. J Appl Toxicol [Internet]. 1999 Nov 1;19(6):421–30. Available from: <URL>.

24. Stammati A, Nebbia C, Angelis I De, Albo AG, Carletti M, Rebecchi C, et al. Effects of malachite green (MG) and its major metabolite, leucomalachite green (LMG), in two human cell lines. Toxicol Vitr [Internet]. 2005 Oct;19(7):853–8. Available from: <URL>.

25. Yadav J, Sahu O, Marwah H. Bioadsorption of dye from textile effluent with surface response methodology. Mater Today Proc [Internet]. 2022;68:937–42. Available from: <URL>.

26. Nayak N, Singha S, Maity JP, Rath PP, Sahoo T, Sahoo TR. Photocatalytic degradation of malachite green dye under solar light irradiation using ZnO and ZnO–TiO_2 nanoparticles. J Mater Sci Mater Electron [Internet]. 2024 Feb 8;35(4):310. Available from: <URL>.

27. Moumeni O, Hamdaoui O, Pétrier C. Sonochemical degradation of malachite green in water. Chem Eng Process Process Intensif [Internet]. 2012 Dec;62:47–53. Available from: <URL>.

28. Ashraf MW, Abulibdeh N, Salam A. Selective removal of malachite green dye from aqueous solutions by supported liquid membrane technology. Int J Environ Res Public Health [Internet]. 2019 Sep 19;16(18):3484. Available from: <URL>.

29. Du LN, Zhao M, Li G, Xu FC, Chen WH, Zhao YH. Biodegradation of malachite green by *Micrococcus* sp. strain BD15: Biodegradation pathway and enzyme analysis. Int Biodeterior Biodegradation [Internet]. 2013 Mar;78:108–16. Available from: <URL>.

30. Lv GY, Cheng JH, Chen XY, Zhang ZF, Fan LF. Biological decolorization of malachite green by *Deinococcus radiodurans* R1. Bioresour Technol [Internet]. 2013 Sep;144:275–80. Available from: <URL>.

31. Kausar A, Iqbal M, Javed A, Aftab K, Nazli Z i H, Bhatti HN, et al. Dyes adsorption using clay and modified clay: A review. J Mol Liq [Internet]. 2018 Apr;256:395–407. Available from: <URL>.

32. Ghibate R, Baaziz M Ben, Taouil R, Senhaji O. Investigation of reacting parameters to improve cationic dye adsorption onto raw pomegranate peel. In 2024. p. 165–74. Available from: <URL>.

33. El-Habacha M, Lagdali S, Dabagh A, Mahmoudy G, Assouani A, Benjelloun M, et al. High efficiency of treated-phengite clay by sodium hydroxide for the Congo red dye adsorption: Optimization, cost estimation, and mechanism study. Environ Res [Internet]. 2024 Oct;259:119542. Available from: <URL>.

34. El-Habacha M, Dabagh A, Lagdali S, Miyah Y, Mahmoudy G, Sinan F, et al. An efficient and adsorption of methylene blue dye on a natural clay surface: Modeling and equilibrium studies. Environ Sci Pollut Res [Internet]. 2023 May 22;31(53):62065–79. Available from: <URL>.

35. Chrachmy M, Ghıbate R, El Hamzaouı N, Lechheb M, Ouallal H, Azrour M. Application of raw moroccan clay as a potential adsorbent for the removal of malachite green dye from an aqueous solution: Adsorption parameters evaluation and thermodynamic study. Mater Res Proc [Internet]. 2024 Apr 15;40:248–59. Available from: <URL>.

36. Ouallal H, Chrachmy M, El Hamzaouı N, Lechheb M, Ghıbate R, El-Marjaouı H, et al. Insight on the natural moroccan clay valorization for malachite green adsorption: Kinetic and isotherm studies. Mater Res Proc [Internet]. 2024 Apr 15;40:273–83. Available from: <URL>.

37. Alshameri A, He H, Zhu J, Xi Y, Zhu R, Ma L, et al. Adsorption of ammonium by different natural clay minerals: Characterization, kinetics and adsorption isotherms. Appl Clay Sci [Internet]. 2018 Jun;159:83–93. Available from: <URL>.

38. Abbou B, Lebkiri İ, Ouaddarı H, Elkhattabi O, Habsaouı A, Lebkırı A, et al. Kinetic and thermodynamic study on adsorption of cadmium from aqueous solutions using natural clay. J Turkish Chem Soc Sect A Chem [Internet]. 2021 May 31;8(2):677–92. Available from: <URL>.

39. Ghibate R, Sabry F, Senhaji O, Taouil R, Touzani M. State of the art of technologies for Zn^{2+} ions removal from industrial effluents with adsorption:

Examination of process parameters (Part I). Int J Innov Res Sci Technol [Internet]. 2016 Jan 4;2(7):39–48. Available from: <URL>.

40. Yadav J, Sahu O. Dye removal of cationic dye from aqueous solution through acid functionalized ceramic. Total Environ Res Themes [Internet]. 2023 Jun;6:100038. Available from: <URL>.

41. Nakhjiri MT, Marandi GB, Kurdtabar M. Poly(AA-co-VPA) hydrogel cross-linked with N-maleyl chitosan as dye adsorbent: Isotherms, kinetics and thermodynamic investigation. Int J Biol Macromol [Internet]. 2018 Oct;117:152–66. Available from: <URL>.

42. Kerrou M, Raada S, Mrani D, Elanssari A. A comparative study of the adsorption of a cationic dye on three substrates. Desalin Water Treat [Internet]. 2023 Nov;311:135–43. Available from: <URL>.

43. Ghibate R, Ben B, Amechrouq A, Taouil R, Senhaji O. The performance of an eco-friendly adsorbent for methylene blue removal from aqueous solution: Kinetic, isotherm, and thermodynamic approaches. J Serbian Chem Soc [Internet]. 2024;89(7–8):1107–21. Available from: <URL>.

44. Dehmani Y, Franco DSP, Georgin J, Lamhasni T, Brahmi Y, Oukhrib R, et al. Comparison of phenol adsorption property and mechanism onto different Moroccan clays. Water [Internet]. 2023 May 16;15(10):1881. Available from: <URL>.

45. Ouallal H, Chrachmy M, Azrour M, Lechheb M, El-Kordy A, Dehmani Y, et al. Study of acid treatment effect of a natural red clay onto physico-chemical and adsorption properties. Desalin Water Treat [Internet]. 2023 Dec;315:96–110. Available from: <URL>.

46. Küçük İ, Üstündağ P. Adsorption performance of acidic modified fly ash: Box–behnken design. J Turkish Chem Soc Sect A Chem [Internet]. 2024 May 15;11(2):699–708. Available from: <URL>.

47. Kerrou M, Bouslamti N, Raada A, Elanssari A, Mrani D. A comparative study of the kinetics and isotherm of adsorption of a cationic dye by different natural wastes. Bourekkadi S, Abouchabaka J, Omari O, Slimani K, editors. E3S Web Conf [Internet]. 2021 Feb 2;234:00059. Available from: <URL>.

48. Serafin J, Dziejarski B. Application of isotherms models and error functions in activated carbon CO_2 sorption processes. Microporous Mesoporous Mater [Internet]. 2023 Apr;354:112513. Available from: <URL>.

49. Ouallal H, Dehmani Y, Moussout H, Messaoudi L, Azrour M. Kinetic, isotherm and mechanism investigations of the removal of phenols from water by raw and calcined clays. Heliyon [Internet]. 2019 May;5(5):e01616. Available from: <URL>.

50. Gürses A, Doğar C, Yalçın M, Açıkyıldız M, Bayrak R, Karaca S. The adsorption kinetics of the cationic dye, methylene blue, onto clay. J Hazard Mater [Internet]. 2006 Apr 17;131(1–3):217–28. Available from: <URL>.

51. Algethami JS, Alhamami MAM, Alqadami AA, Melhi S, Seliem AF. Magnetic hydrochar grafted-chitosan for enhanced efficient adsorption of malachite green dye from aqueous solutions: Modeling, adsorption behavior, and mechanism analysis. Int J Biol Macromol [Internet]. 2024 Jan;254:127767. Available from: <URL>.

52. Hussien Hamad MTM. Optimization study of the adsorption of malachite green removal by MgO nano-composite, nano-bentonite and fungal immobilization on active carbon using response surface methodology and kinetic study. Environ Sci Eur [Internet]. 2023 Apr 17;35(1):26. Available from: <URL>.

53. Bensalah J, Habsaoui A, Abbou B, Kadiri L, Lebkiri I, Lebkiri A, et al. Adsorption of the anionic dye methyl orange on used artificial zeolites: Kinetic study and modeling of experimental data. Mediterr J Chem [Internet]. 2019 Nov 18;9(4):311–6. Available from: <URL>.

54. Ouaddari H, Abbou B, Lebkiri I, Habsaoui A, Ouzzine M, Fath Allah R. Removal of methylene blue by adsorption onto natural and purified clays: Kinetic and thermodynamic study. Chem Phys Impact [Internet]. 2024 Jun;8:100405. Available from: <URL>.

55. Ghibate R, Kerrou M, Chrachmy M, Baaziz M Ben, Taouil R, Senhaji O. Utilizing agricultural waste for sustainable remediation of textile dyeing effluents. Ecol Eng Environ Technol [Internet]. 2024 Jul 1;25(7):369–78. Available from: <URL>.

56. Wei W, Wang B, Huang X, Zhou Z, Yan Y, Li L, et al. Potassium salts activated lignin-based biochar as an effective adsorbent for malachite green adsorption. Int J Biol Macromol [Internet]. 2024 Oct;277:134209. Available from: <URL>.

57. Ghibate R, Ben Baaziz M, Chrachmy M, Kerrou M, Taouil R, Senhaji O. Production of new activated carbon from agricultural waste and its use as an eco-friendly solution for removing copper ions from industrial effluents. Ecol Eng Environ Technol [Internet]. 2024 Oct 1;25(10):96–106. Available from: <URL>.

58. Tahir SS, Rauf N. Removal of a cationic dye from aqueous solutions by adsorption onto bentonite clay. Chemosphere [Internet]. 2006 Jun;63(11):1842–8. Available from: <URL>.

59. Zaoui F, Zohra Choumane F, Hakem A. Malachite green dye and its removal from aqueous solution by clay-chitosane modified. Mater Today Proc [Internet]. 2022;49:1105–11. Available from: <URL>.

60. Moustafa MT. Preparation and characterization of low-cost adsorbents for the efficient removal of malachite green using response surface modeling

and reusability studies. Sci Rep [Internet]. 2023 Mar 18;13(1):4493. Available from: <URL>.

61. Moumen A, Belhocine Y, Mechati F, Karout M, Charime D, Boultif W, et al. Spectral, isotherm, kinetic, and thermodynamic studies of malachite green dye adsorption from aqueous solutions onto low-cost treated kaolin. Phys Chem Res [Internet]. 2024 Mar 1;12(1):47–60. Available from: <URL>.

62. Tian L, Zhang J, Shi H, Li N, Ping Q. Adsorption of malachite green by diatomite: Equilibrium isotherms and kinetic studies. J Dispers Sci Technol [Internet]. 2016 Jul 2;37(7):1059–66. Available from: <URL>.

63. Baran E, Acemioğlu B. Competitive removal of malachite green and rhodamine B using clinoptilolite in a two-dye system. Clays Clay Miner [Internet]. 2016 Jun 1;64(3):299–313. Available from: <URL>.

64. Imessaoudene A, Cheikh S, Bollinger JC, Belkhiri L, Tiri A, Bouzaza A, et al. Zeolite waste characterization and use as low-cost, ecofriendly, and sustainable material for malachite green and methylene blue dyes removal: Box–behnken design, kinetics, and thermodynamics. Appl Sci [Internet]. 2022 Jul 28;12(15):7587. Available from: <URL>.

65. Hashem AA, Mahmoud SA, Geioushy RA, Fouad OA. Adsorption of malachite green dye over synthesized calcium silicate nanopowders from waste materials. Mater Sci Eng B [Internet]. 2023 Sep;295:116605. Available from: <URL>.

JOTCSA Journal of the Turkish Chemical Society Section: A Chemistry

TURKISH CHEMICAL SOCIETY

Synthesis and Characterisation of Novel Palladium(II) Isatin-3-Thiosemicarbazone Complexes with Phosphine and Phenanthroline Ligands: In Vitro Evaluation Against Cancer Cell Lines and Bacterial Strains

Ali H. Al-Obaidi[1], Luma A. Al-Doori[2], Ahmed A. Irzoqi[2], Mohanad Y. Al-Radeef[3*]

[1]Tikrit University, College of Pharmacy, Pharmaceutical Chemistry Department, Tikrit, 34001, Iraq.
[2]Tikrit University, College of Education for Pure Science, Chemistry Department, Tikrit, 34001, Iraq.
[3]Tikrit University, College of Pharmacy, Clinical Pharmacy Department, Tikrit, 34001, Iraq.

Abstract: In this study, three new palladium (II) complexes with isatin-3-thiosemicarbazone (ITC) were prepared by reacting Pd(II) with ITC and phosphine or diamine ligands. Characterisation was done using CHN analysis, molar conductivity, FTIR spectroscopy, and ^{1}H, ^{13}C, and ^{31}P NMR spectroscopy. All analyses confirmed that the complexes exhibit a square planar structure around the Pd^{2+} ion. The ITC ligand displayed a bidentate coordination mode, binding through nitrogen and sulphur atoms. In vitro biological activity studies revealed excellent anti-ovarian cancer potential. Notably, the complex $(Pd(ITC)(Phen))Cl_2$ demonstrated only 5% cell survival at a 400 µM concentration, while the other two complexes, $(Pd(ITC)_2)Cl_2$ and $(Pd(ITC)(PPh_3)Cl)Cl$, did not exceed 10%. These results illustrate the strong ability of these complexes to inhibit cancer cell growth in vitro. Additionally, the three synthesised complexes demonstrated clear antibacterial activity against four bacterial strains: two Gram-positive (*Streptococcus faecalis* and *Staphylococcus aureus*) and two Gram-negative (*E. coli* and *Pseudomonas aeruginosa*). The activity was concentration-dependent, decreasing as the concentration lowered. The complex $(Pd(ITC)(Phen))Cl_2$ exhibited the highest antibacterial activity, particularly against Gram-positive bacteria, followed by $(Pd(ITC)(PPh_3)Cl)Cl$ and $(Pd(ITC)_2)Cl_2$. These findings indicate the possible development of these complexes as therapeutic agents with anticancer and antibacterial properties, particularly in addressing bacterial resistance to conventional antibiotics.

Keywords: Pd(II), (ITC), Cyclic nitrogen, Anti-ovarian cancer activity.

Submitted: February 25, 2025. **Accepted:** June 12, 2025.

Cite this: Al-Obaidi AA, Al-Doori LA, Irsoqi AA, Al-Radeef MY. Synthesis and Characterisation of Novel Palladium(II) Isatin-3-Thiosemicarbazone Complexes with Phosphine and Phenanthroline Ligands: In Vitro Evaluation Against Cancer Cell Lines and Bacterial Strains. JOTCSA. 2025;12(3): 181-8.

DOI: https://doi.org/10.18596/jotcsa.1646336

***Corresponding author's E-mail:** mohanadyasir@tu.edu.iq

1. INTRODUCTION

Thiosemicarbazones (TSCs) are significant compounds in coordination chemistry due to their strong metal-chelating capabilities and notable biological activities (1-3), particularly in inhibiting ribonucleotide reductase (RR), an essential enzyme for DNA synthesis (4). These compounds exhibit antiviral and antibacterial properties (5), are utilised in HIV detection (6), and have shown antimalarial effects (7). Their derivatives demonstrate a range of biological activities, including anti-tumour, anti-cancer, and anti-inflammatory effects (8). Thiosemicarbazone (TSC) compounds are among the most prominent ligands used in coordination chemistry. They are typically synthesised as Schiff bases through condensation reactions between thiosemicarbazide and suitable carbonyl compounds and are regarded as effective coordinating agents due to the presence of nitrogen and sulphur donor atoms in their structures (9). The inclusion of a thiol group further classifies them as part of a vital ligand family capable of binding to metals through single, double, or bridging bonds (10,11).

These compounds are recognised for forming stable complexes with transition metals (12). In "isatin-thiosemicarbazone" derivatives, the nitrogen, sulphur, and carbonyl oxygen atoms function as active donor sites. Thiosemicarbazide has also been extensively researched for its bonding capabilities

with various cations via its sulphur or nitrogen atoms (13–16).

Isatin-thiosemicarbazones hold particular significance due to their physiological activity, attributed to the additional oxygen donor atoms from the indole ring, which introduce multiple coordination sites within the molecular framework (17). This structural feature has garnered substantial interest in coordination chemistry by facilitating diverse coordination modes with metal ions (18). Previous studies have reported complexes of these ligands with triphenylphosphines and amines (19), while those involving palladium or mercury have demonstrated promising performance in hydrogen storage applications (20-22).

Additionally, several precursor complexes have been studied to evaluate their potential as anticancer agents and their hydrogen absorption capabilities (23). Based on this, the present study aims to prepare new palladium(II) complexes of isatin-thiosemicarbazone compounds with various coordinating ligands, such as triphenylphosphine (PPh_3) and 1,10-phenanthroline (Phen). The focus is on the formation of stable complexes and their characterisation using different techniques. The study also investigates their effects on two cancer cell lines, MCF-7 and 518A2, as well as on four different bacterial strains: two Gram-positive (*Streptococcus faecalis* and *Staphylococcus aureus*) and two Gram-negative (*Escherichia coli* and *Pseudomonas aeruginosa*).

2. EXPERIMENTAL SECTION

2.1. Materials and Instrumentation

All chemicals, reagents, and solvents used to manufacture compounds were supplied and employed without purification.

The melting point of the prepared complexes was recorded using an automatic melting point device (SMP30). The molar conductivity of a freshly prepared 10^{-3} M DMSO solution was noted. The complexes were measured with the Starter 3100c digital conductivity meter. The infrared spectra of the complexes were recorded as KBr tablets using the Shimadzu FTIR 8400s spectrometer (400-4000 cm^{-1}) at the Tikrit University, College of Pure Science in Iraq. Microanalyses for carbon, hydrogen, nitrogen and sulphur were carried out using an Elementar vario El III CHN elemental analyser. Nuclear magnetic resonance spectra were obtained on the Bruker 400 MHz spectrometer using DMSO-d6 as the solvent at the University of Tehran, College of Science.

2.2. Preparation of Ligand (ITC)

The ligand (ITC) was synthesised using a conventional method described in reference (24). Thiosemicarbazide (0.55 g, 7.1 mmol) was dissolved in 10 mL of an appropriate solvent. A solution of isatin (0.99 g, 6 mmol) was prepared in 10 mL of ethanol and added to the mixture, which was then heated in a water bath at 50 °C after adding two to three drops of glacial acetic acid as a catalyst. The reaction mixture was refluxed for one hour and subsequently allowed to cool. The resulting yellow precipitate was separated by filtration, washed with cold ethanol, and dried in a hot-air oven at 90 °C. A yellow crystalline compound with the molecular formula $C_9H_8N_4OS$ was obtained, yielding 1.88 g (83%). Elemental analysis was performed, and the theoretical values for carbon, hydrogen, nitrogen, and sulphur were calculated as follows: C = 49.77%, H = 4.12%, N = 26.00%, S = 14.56%. The experimentally found values were: C = 49.55%, H = 2.960%, N = 26.45%, S = 15.07%.

2.3. Synthesis of $(Pd(ITC)_2)Cl_2$

A solution of $PdCl_2$ (1.793 g, 10 mmol) in 99% ethanol (20 mL) was slowly added to a solution of HITC (3.155 g, 10 mmol) in 99% ethanol (20 mL). The mixture was stirred for two hours, resulting in the formation of a yellow suspension. $(Pd(ITC)_2)Cl_2$ (1) appeared as an orange solid with a yield of 0.7272g (90.0% yield). Elemental analysis yielded: C, 33.91; H, 2.64; N, 22.60; S, 12.93; found: C, 34.22; H, 2.97; N, 22.26; S, 12.49. Conductivity measured at 67.3 $\Omega^{-1}\cdot cm^2\cdot mol^{-1}$. IR (KBr, cm-1): 3417s (NH), 3265s (C-H), 3145m (C=S), 1699s (C=O), 1606s (C=N),1344s (C=S),1504s (N-H). 1H-NMR (DMSO-d6): 12.37 (S, 1H, NH isatin), 9.02 (S, 1H, NH2), 8.63 (S, 1H, NH2), 7.64 (d, 1H, Ha), 7.36 (t, 1H, Hc), 7.09 (t, 1H, Hb), 6.91 (d, 1H, Hd). 13C-{1H} NMR: δc, S, 179.3 (C=S), δc, S, 166.1 (C=O), δc, 142.5 (C-NH), δc, 134.2 (C=N), δc, 131.1 -117.2 (Ph-C). Melting point: 262 ℃.

2.4. Synthesis of $(Pd(ITC)(Phen))Cl_2$ and $(Pd(ITC)(PPh_3)Cl)Cl$ Complexes

A solution of Na_2PdCl_4 (1.81 mmol, 0.5 g) in 10 mL of absolute ethanol was added to a solution of Phen (1.81 mmol, 0.359 g) in 10 mL of absolute ethanol. The mixture was stirred for an hour at 20°C, resulting in a white precipitate. To this precipitate, a solution of ITC (1.81 mmol, 0.399 g) in 10 mL of absolute ethanol was added. The mixture was stirred for two hours at 20 °C, yielding a light yellow precipitate. The precipitate was filtered, washed with cold ethanol, and dried under reduced pressure, yielding $(Pd(ITC)(Phen))Cl_2$ (2), a pale yellow solid with a yield of 1.231 g (97%). Calculated elemental analysis: C, 38.77; H, 2.00; N, 20.87; S, 7.96; found: C,39.17; H,2.30; N,20.15; S,7.43. Molar conductivity: 76.4 Ω-1.cm^2.$mol^{-1.}$ IR (KBr, cm^{-1}): 3247 m (NH), 3419 w (NH2), 3051 w (=C–H), 1679 s (C=O), 1614 s, 1583 s, 1487 m (C=N), 1346 m (C=S), 854 m. 1H-NMR (DMSO-d_6):11.21 (bs, 1 H, NH), 9.16 (s, 1 H, NH2), 8.86 (s, 1 H, NH2), 9.27 (d, 2 H, H1 phen), 8.97 (d, H3 phen), 8.13 (s, 2 H, H4 phen), 8.18 (m, 2 H, H2 phen), 7.66 (d, 1 H, Ha), 7.37 (t, 1 H, Hc), 7.10 (t, 1 H, Hb), 8.97 (d, 1 H, Hd). 13C-{1H} NMR (DMSO-d6): δ178.98 (C=S), 164.21(C=O), 156.55(C=O)ITC, 141.77 (C1, phen), 139.31(C=N) ITC, 134.68–116.92 (aromatic ITC, phen). Melting point: 285-288 °C.

The solution of (Na_2PdCl_4) (2.302 mmol, 0.0474g) in 10 mL of chloroform was slowly added to the solution of (ITC) (2.302 mmol, 0.0507 g) in 10 mL of chloroform, and the mixture was allowed to ascend for two hours, resulting in the formation of a white precipitate. A solution of a (20 mmol) equivalent of PPh_3 in chloroform (51 mL) was then added to the previous mixture and refluxed for three more hours. The pale yellow or white precipitate was collected and dried at room temperature. $(Pd(ITC)(PPh_3))Cl_2$ (3) Orange solid, yield (2.817 g, 80%). Calculated

elemental analysis: C, 48.27; H, 3.35; N, 9.79; S, 5.60; found: C, 48.70; H, 3.69; N, 9.65; S, 5.48. Molar conductivity (30.8 $\Omega^{-1}.cm^2.mol^{-1}$). IR (KBr, cm^{-1}): 3417 m (NH2), 3272 m (NH), 3049 m (=C–H), 2977 w (C–H); 1677 s (C=O), 1614 s (C=N), 1429 s (P–Ph), 1477 m (Ph-Ph), 1344 w (C-S), 1095 m (P–C), 690 s. ^{1}H-NMR (δ ppm, J Hz, DMSO-d_6): 11.20 (s, 1H, NH), 9.04 (s, 1H, NH2), 8.69 (s, 1H, NH2), (7.68–7.50) (m, 15H, PPh_3), 7.67 (d, 1H, Ha), 7.36 (t, 1H, Hc), 7.10 (t, 1H, Hb), 6.940 (d, 1H, Hd). ^{31}P-{^{1}H}NMR (δ ppm, JHz, DMSO-d_6): 30.62. Melting point: 279–282 ◦C.

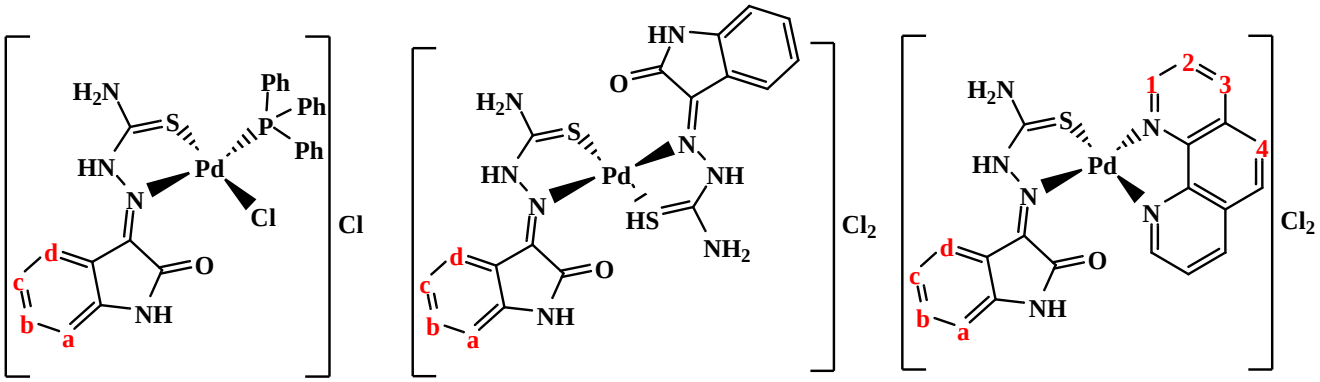

(3) (1) (2)

Figure 1: The prepared complexes.

2.5. Evaluation of the Bacterial Activity of the Prepared Complexes

The bacterial (biological) activity of the prepared complexes was evaluated on four types of bacteria: two Gram-positive and two Gram-negative strains, using the agar well diffusion method. (25) The bacterial isolates were identified by the Department of Life Sciences at the College of Science, Tikrit University, and they are: *Pseudomonas aeruginosa* (Gram-negative), *Escherichia coli* (Gram-negative), *Staphylococcus aureus* (Gram-positive), and *Streptococcus faecalis* (Gram-positive).

The complex solutions were prepared using DMSO solvent at concentrations of (10^{-1}, 10^{-3}, 10^{-5} x 1 M). Next, the culture medium was prepared by dissolving 38 grams of nutrient agar in 1 litre of distilled water and placing it in a conical flask. The mixture was stirred thoroughly and heated until the agar (a gelatinous substance used as a medium for bacterial growth) was completely dissolved. Afterwards, the medium was sterilized in an autoclave at 121 °C and 15 bars for 15 minutes. After sterilisation, the medium was poured into Petri dishes and left to solidify.

Subsequently, 3 to 5 bacterial swabs were placed on the prepared medium and incubated for 24 hours at 37 °C. For evaluating biological activity, a second medium was prepared by dissolving 53.5 grams of Mueller-Hinton agar in 1 litre of distilled water. The medium was sterilised in an autoclave at 121 °C and 15 bars for 15 minutes.

After sterilisation, the medium was poured into Petri dishes and allowed to solidify. A quantity of activated bacteria was collected using a swab and spread evenly over the solidified Mueller-Hinton agar. The plate was left for 30 minutes to facilitate absorption, and then wells were created using a sterile 5 mm diameter punching tool. Four wells were formed, and 1 mL of each prepared compound solution at varying concentrations was added to the wells. All Petri dishes were incubated for 24 hours. The inhibition zones were measured to assess the effectiveness of the compounds in inhibiting bacterial growth (26).

3. RESULTS AND DISCUSSION

Molar conductivity of the complexes exhibited molar conductivity values in DMSO at (25 °C, 10^{-3} M) within the range of (67.3 - 76.4 $\Omega^{-1}\cdot cm^2\cdot mol^{-1}$) for $(Pd(ITC)_2)Cl_2$ and $(Pd(ITC)(Phen))Cl_2$ respectively, indicating that the solutions of these complexes are 1:2 electrolytes. On the other hand, the complex $(Pd(ITC)PPh_3)Cl)Cl$ (3) showed a value of (30.8 $\Omega^{-1}\cdot cm^2\cdot mol^{-1}$), suggesting that the solution of this complex is a 1:1 electrolyte (27,28).

The FTIR spectrum of the free ligand HITC exhibited vibrational bands at 3419, 3265/3174, 1679, 1614, and 1346 cm^{-1}, corresponding to ν(N-H), ν(NH_2), ν(C=O), ν(C=N), and ν(C=S) respectively (28,29). The bands associated with the NH_2 groups in the prepared complexes were slightly shifted from their positions in the free ligand, indicating no coordination of the NH_2 nitrogen groups with the metal ions. Additionally, NH group bands in the prepared complexes appeared in the range of 8-9, along with a shift of the ν(CS) group bands to lower values, within the range of 1313-1334 cm^{-1}, confirming the coordination of the ligand through the sulphur atom of the thionate group. All prepared complexes exhibited sharp and strong bands in the range of 1658-1697 cm^{-1}, attributed to ν(C=O), while the bands in the range of 1512-1583 cm^{-1} were assigned to the vibration of the ν(C=N) group (28,29).

The ^{1}H-NMR spectrum of the ITC ligand revealed a singlet at (δH=13.93 ppm, 1H) and (δH=11.37 ppm, 1H), corresponding to the NH protons in the isatin and hydrazone groups, respectively. Two doublet signals appeared at (δH=7.88ppm, 2H, 3JH-H = 7.70 Hz) and (δH=7.67ppm, 1H, ^{3}JH-H = 7.59 Hz), which were attributed to the He and Ha protons, respectively. A triplet signal was observed at

(δH=7.60ppm, 3H, 3JH-H = 7.92 Hz), corresponding to the Hf and Hg protons. Additionally, two triplet signals appeared at (δH=7.38 ppm, 1H, ^{3}JH-H =7.13 Hz) and (δH=7.10 ppm, 1H, ^{3}JH-H =7.68 Hz), assigned to the Hc and Hb protons, respectively. A doublet signal was observed at (δH=6.95ppm, 1H, ^{3}JH-H = 7.88 Hz) for the Hd proton (28,30).

The ^{13}C-NMR spectrum of ITC showed signals at (δC=200.70 ppm) and (δC=175.95 ppm), corresponding to the (C=O) carbons in the benzoyl and isatin groups, respectively. Signals were also observed in the range of (δC=158.05-159.02 ppm) for the atoms (C7, C1, C8, and C11) in sequence and (δC=142.92 ppm) assigned to the (C5) carbon.

The ^{1}H-NMR spectrum of the complex $(Pd(ITC)_2)Cl_2$ showed a singlet at (δH = 12.37ppm) with an integration of one proton corresponding to the NH group of thiosemicarbazone. The spectrum also showed a singlet at (δH = 11.23 ppm) with an integration of one proton corresponding to the NH group of isatin. Two singlets appeared at (δH=9.02 ppm) and (δH=8.63 ppm) for the NH_2 group, indicating unequal protonation of the amine group, with one proton for each. A doublet signal appeared at (δH=7.64 ppm) for the Ha proton, integrating one proton, and a triplet at (δH=7.36 ppm) integrating one proton for the Hc proton. The spectrum showed a triplet at (δH=7.09 ppm) integrating one proton for the Hb proton. A doublet signal also appeared at (δH=6.92 ppm) integrating one proton for the Hd proton (28,30).

The ^{1}H-NMR spectrum of complex (**1**) showed a singlet at (δH=12.54 ppm) with a one proton integration for the NH group of thiosemicarbazone. A singlet at (δH=11.21 ppm) with a one proton integration corresponded to the NH group of isatin. Two singlets at (δH=9.16 ppm) and (δH=8.86 ppm) were assigned to the NH_2 group, indicating unequal protonation of the amine group, with one proton for each. The spectrum also showed a signal for the ligand (Phen), with a doublet at (δH=9.27 ppm) for the H1 proton, integrating two protons, and another doublet at (δH=8.97 ppm) for the H3 proton, integrating two protons. The spectrum also showed a singlet at (δH=8.31 ppm) for the H4 proton, integrating two protons, and a multiplet at (δH=8.18 ppm) for the H2 proton, integrating two protons. A doublet appeared at (δH=7.66 ppm) for the Ha proton, integrating one proton, and a triplet at (δH=7.37 ppm) for the Hc proton, integrating one proton. A triplet at (δH=7.10 ppm) for the Hb proton, integrating one proton, and a doublet at (δH=6.93 ppm) for the Hd proton, integrating one proton, were also observed.

The ^{1}H-NMR spectra of complexes (2-5) showed various signals for both the ligand (ITC) and the corresponding phosphine. A singlet at (δH=12.49 ppm) with one proton integration corresponded to the NH group of thiosemicarbazone. The spectrum also showed a singlet at (δH=11.20 ppm) with one proton integration for the NH group of isatin, and two singlets at (δH=9.04 ppm) and (δH=8.69 ppm) for the NH_2 group, indicating unequal protonation of the amine group, with one proton for each. In the spectra of complex (2), two multiplets appeared at (δH=7.62 ppm) and (δH=7.50 ppm), integrating 15 protons, attributed to the phenyl rings of (PPh_3). In the spectra of complex (3), two multiplets appeared at (δH=7.69 ppm) and (δH=7.56 ppm), integrating approximately 11 protons corresponding to the phenyl rings of dppe, with proton Ha among them (28,30).

3.1. Anti-Cancer Activity of $(Pd(ITC)(PPh_3)Cl_2)$

The cytotoxic activity of the complex $(Pd(ITC)(PPh_3)Cl_2)$ was evaluated using the MTT assay against two human cancer cell lines: MCF-7 (breast adenocarcinoma) and 518A2 (melanoma), at a concentration of 0.01 µm. The results showed that the complex exhibited significant inhibitory effects against both cell lines (31,32).

Against the MCF-7 cell line, $(Pd(ITC)(PPh_3)Cl_2)$ demonstrated an IC_{50} value of 15.43 µM, indicating good cytotoxic potential, although it was less effective than cis-platin (IC_{50} = 4.45 ± 0.04 µM).

Similarly, against the 518A2 cell line, the same complex exhibited an IC_{50} value of 16.93 µM, compared to cis-platin with an IC_{50} of 1.45 ± 0.04 µm.

These findings suggest that $(Pd(ITC)(PPh_3)Cl_2)$ possesses promising anticancer activity, particularly among the tested Pd(II) complexes, though it remains less potent than cis-platin (33).

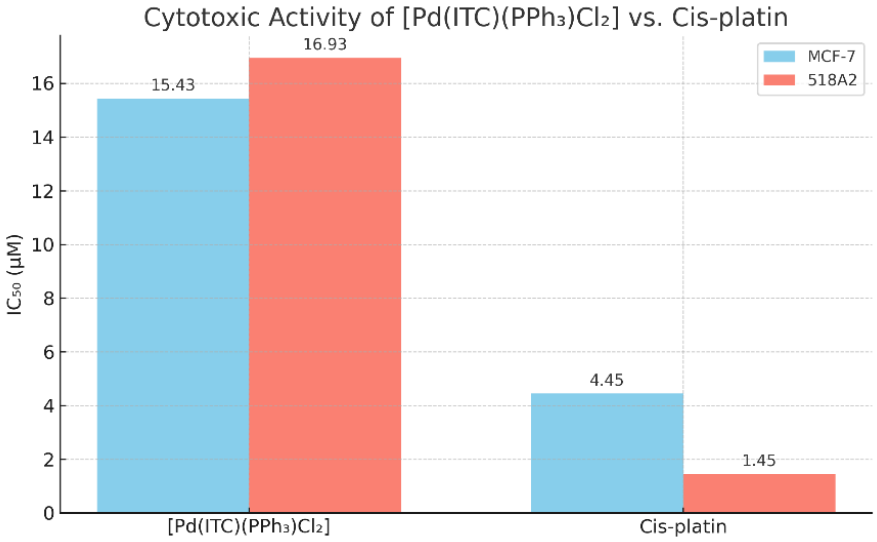

Figure 2: Comparison of IC_{50} Values for $(Pd(ITC)(PPh_3)Cl_2)$ and Cisplatin Against MCF-7 and 518A2 Cell Lines.

3.2. Biological Study

The antibacterial activity of three synthesised complexes $(Pd(ITC)_2)Cl_2$, $(Pd(ITC)(Phen))Cl_2$, and $(Pd(ITC)(PPh_3)Cl)Cl$ was assessed against four bacterial strains: two Gram-positive (*Streptococcus faecalis* and *Staphylococcus aureus*) and two Gram-negative (*Escherichia coli* and *Pseudomonas aeruginosa*). This evaluation utilised the disc diffusion method at various concentrations (10^{-3}, 10^{-4}, and 10^{-5} g/mol) for each complex, with DMSO serving as the solvent. The findings indicated that the antibacterial effectiveness of these complexes was distinctly concentration-dependent; inhibition zones decreased as the concentration lowered, and no activity was noted at the lowest concentration (10^{-5} g/mol).

The complex $(Pd(ITC)_2)Cl_2$ exhibited moderate activity against all tested bacterial strains at the highest concentration (10^{-3} g/mol), showing inhibition zones from 21 mm for Gram-positive bacteria up to 31 mm for Gram-negative bacteria. However, this activity dropped significantly at lower concentrations. In contrast, $(Pd(ITC)(Phen))Cl_2$ displayed the highest antibacterial activity among the tested complexes, particularly against Gram-positive bacteria, achieving an inhibition zone of 36 mm against *S. aureus* at the maximum concentration. It also revealed considerable effectiveness against Gram-negative bacteria. The complex $(Pd(ITC)(PPh_3)Cl)Cl$ demonstrated consistent effectiveness against all examined strains, with inhibition zones ranging from 27 mm to 32 mm at the highest concentration, followed by a gradual reduction at lower concentrations.

This may be attributed to the rigid and planar structure of Phen, which may allow better interaction with cellular structures compared to the structure of PPh_3, where the phenyl rings increase steric hindrance (23).

These results indicate that the synthesised complexes exhibit promising biological activity as antibacterial agents, particularly at higher concentrations. This suggests their potential for future development as pharmaceutical compounds, especially in light of the growing bacterial resistance to conventional antibiotics (34-36).

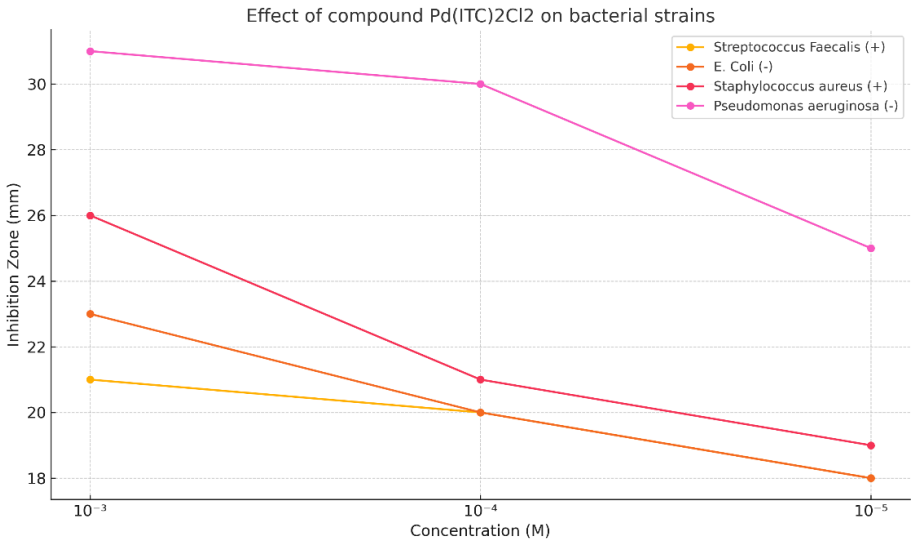

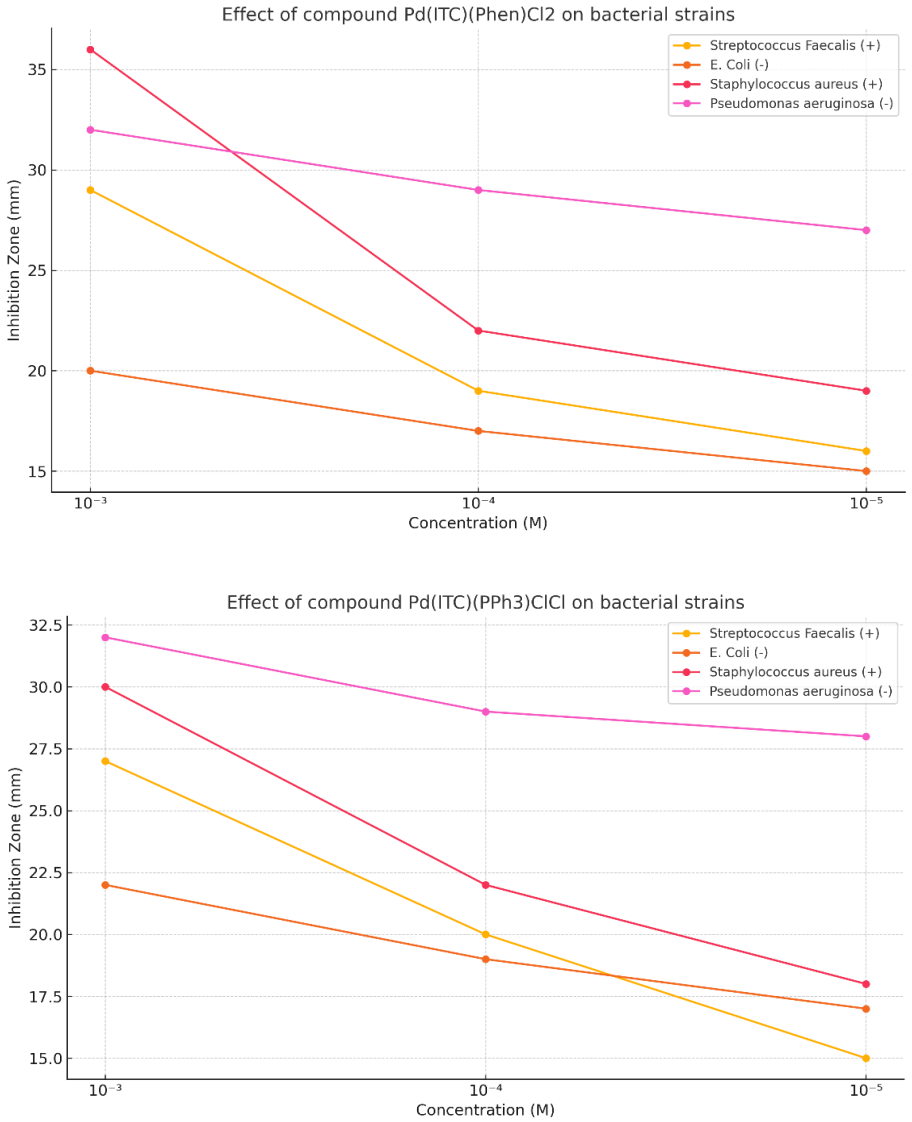

Figure 3: Antibacterial Activity of Palladium(II) Isothiocyanate Complexes Against Various Bacterial Strains at Different Concentrations.

3.3. Future Implications

These findings further explore the action mechanisms of such compounds and their efficacy for cell lines of other tumours. Furthermore, some studies by (36) allow us to suggest that treating certain diseases with palladium(II) complexes combined with other therapeutic agents can enhance effectiveness with reduced toxicity, which could be investigated in future studies involving our synthesised compounds.

These results have therefore unravelled the potential of such complexes in developing novel therapeutic agents. Further preclinical studies, including toxicity profiling, mechanistic studies, and pharmacokinetics, could help refine and optimise compounds for clinical applications. In this respect, the high anti-ovarian cancer activity suggests that this compound is a good candidate for targeted synthesis as a chemotherapeutic drug, playing a significant role in improving cancer treatment outcomes.

4. CONCLUSION

Because most cancers are preventable, it is possible to create new and suitable pharmacological compounds in this study. The biological and antioxidant activity of the produced compounds was good. The preparation was done effortlessly and confidently due to the favourable proportion of the compounds, as revealed in the research.

5. CONFLICT OF INTEREST

The authors declare no conflict of interest to declare.

6. REFERENCES

1. Aziz KN, Ahmed KM, Omer RA, Qader AF, Abdulkareem EI. A review of coordination compounds: Structure, stability, and biological significance. Rev Inorg Chem [Internet]. 2025 Mar 1;45(1):1–19. Available from: <URL>.

2. Trudu F, Amato F, Vaňhara P, Pivetta T, Peña-Méndez EM, Havel J. Coordination compounds in cancer: Past, present and perspectives. J Appl Biomed [Internet]. 2015 May 1;13(2):79–103. Available from: <URL>.

3. Kumar Singh V, Kumar Singh V, Mishra A, Varsha, Abha Singh A, Prasad G, et al. Recent advancements in coordination compounds and their potential clinical application in the management of diseases: An up-to-date review. Polyhedron [Internet]. 2023 Sep 1;241:116485. Available from: <URL>.

4. Bai XG, Zheng Y, Qi J. Advances in thiosemicarbazone metal complexes as anti-lung cancer agents. Front Pharmacol [Internet]. 2022 Sep 27;13:1018951. Available from: <URL>.

5. Korkmaz G. A review of recent research on the antimicrobial activities of thiosemicarbazone-based compounds. J New Results Sci [Internet]. 2024 Apr 30;13(1):61–83. Available from: <URL>.

6. Farghaly TA, Abbas EMH, Abd-Elghaffar HS, Elsayed MA, Elnaggar DH, El-Sayed AF, et al. Synthesis, characterization, molecular docking, pharmacokinetics, and molecular dynamics of new bis-thiazoles based on bis-thiosemicarbazone as anti-coxsackievirus. Sci Rep [Internet]. 2024 Nov 26;14(1):29378. Available from: <URL>.

7. Savir S, Wei ZJ, Liew JWK, Vythilingam I, Lim YAL, Saad HM, et al. Synthesis, cytotoxicity and antimalarial activities of thiosemicarbazones and their nickel (II) complexes. J Mol Struct [Internet]. 2020 Jul 5;1211:128090. Available from: <URL>.

8. Gupta S, Singh N, Khan T, Joshi S. Thiosemicarbazone derivatives of transition metals as multi-target drugs: A review. Results Chem [Internet]. 2022 Jan 1;4:100459. Available from: <URL>.

9. Leovac VM, Novaković SB. Versatile coordination chemistry of thiosemicarbazide and its non-Schiff base derivatives. J Mol Struct [Internet]. 2024 Oct 15;1314:138721. Available from: <URL>.

10. Bjørklund G, Crisponi G, Nurchi VM, Cappai R, Buha Djordjevic A, Aaseth J. A review on coordination properties of thiol-containing chelating agents towards mercury, cadmium, and lead. Molecules [Internet]. 2019 Sep 6;24(18):3247. Available from: <URL>.

11. Mucha P, Skoczyńska A, Małecka M, Hikisz P, Budzisz E. Overview of the antioxidant and anti-inflammatory activities of selected plant compounds and their metal ions complexes. Molecules [Internet]. 2021 Aug 12;26(16):4886. Available from: <URL>.

12. Aly AA, Abdallah EM, Ahmed SA, Rabee MM, Bräse S. Transition metal complexes of thiosemicarbazides, thiocarbohydrazides, and their corresponding carbazones with Cu(I), Cu(II), Co(II), Ni(II), Pd(II), and Ag(I)—A Review. Molecules [Internet]. 2023 Feb 14;28(4):1808. Available from: <URL>.

13. Haribabu J, Srividya S, Mahendiran D, Gayathri D, Venkatramu V, Bhuvanesh N, et al. Synthesis of palladium(II) complexes via michael addition: Antiproliferative effects through ROS-mediated mitochondrial apoptosis and docking with SARS-CoV-2. Inorg Chem [Internet]. 2020 Dec 7;59(23):17109–22. Available from: <URL>.

14. Irzoqi AA, Salih MM, Jirjes HM, Mensoor MK. Synthesis, characterization, and antibacterial activity of complexes of Hg(II) with mixtures of 3-hydrazonoindolin-2-one and diphosphine, or diimine ligands. Russ J Gen Chem [Internet]. 2020 Jun 22;90(6):1069–73. Available from: <URL>.

15. Al-Jibori SA, Irzoqi AA, Al-Saraj EGH, Al-Janabi ASM, Basak-Modi S, Ghosh S, et al. Formation of ortho-cyano-aminothiophenolate ligands with versatile binding modes via facile carbon–sulfur bond cleavage of 2-aminobenzothiazoles at mercury(II) centres. Dalt Trans [Internet]. 2015 Aug 4;44(32):14217–9. Available from: <URL>.

16. Al-Jibori SA, Irzoqi AA, Al-Janabi ASM, Al-Nassiry AIA, Basak-Modi S, Ghosh S, et al. Synthesis, structure and reactivity with phosphines of Hg(II) *ortho*-cyano-aminothiophenolate complexes formed *via* C–S bond cleavage and dehydrogenation of 2-aminobenzothiazoles. Dalt Trans [Internet]. 2022 May 24;51(20):7889–98. Available from: <URL>.

17. Kazemi Z, Rudbari HA, Moini N, Momenbeik F, Carnamucio F, Micale N. Indole-containing metal complexes and their medicinal applications. Molecules [Internet]. 2024 Jan 18;29(2):484. Available from: <URL>.

18. Adhikari HS, Garai A, Yadav PN. Synthesis, characterization, and anticancer activity of chitosan functionalized isatin based thiosemicarbazones, and their copper(II) complexes. Carbohydr Res [Internet]. 2023 Apr 1;526:108796. Available from: <URL>.

19. Mohsin N, Khalid S, Rasool N, Aman L, Kanwal A, Imran M. Metallo-organic complexes containing transition metals; synthetic approaches and pharmaceutical aspects. Chempluschem [Internet]. 2025 May 20;90(5):e202400748. Available from: <URL>.

20. Qureshi F, Yusuf M, Ahmed S, Haq M, Alraih AM, Hidouri T, et al. Advancements in sorption-based materials for hydrogen storage and utilization: A comprehensive review. Energy [Internet]. 2024 Nov 15;309:132855. Available from: <URL>.

21. Al-Doori LA, Al-Jibori SA, Al-Janabi ASM, Alheety MA, Irzoqi AA. Synthesis, spectroscopic and hydrogen storage studies of mono or bimercury(II) mixed ligand complexes of amines with 2-cyanoamino thiophenolate ligand. J Mol Struct [Internet]. 2023 Nov 5;1291:135992. Available from: <URL>.

22. Irzoqi AA, Salman FA, Alasadi YK, Alheety MA. Synthesis and structural characterization of palladium(II) mixed-ligand complexes of *N*-(Benzothiazol-2-yl)benzamide and 1,2-Bis(diphenylphosphino)ethane. Inorg Chem [Internet]. 2021 Dec 20;60(24):18854–8. Available from: <URL>.

23. Al-Doori LA, Irzoqi AA, Jirjes HM, AL-Obaidi AH, Alheety MA. Zn(II)-isatin-3-thiosemicarbazone complexes with phosphines or diamines for hydrogen storage and anticancer studies. Inorg

Chem Commun [Internet]. 2022 Jun 1;140:109454. Available from: <URL>.

24. Banerjee D, Yogeeswari P, Bhat P, Thomas A, Srividya M, Sriram D. Novel isatinyl thiosemicarbazones derivatives as potential molecule to combat HIV-TB co-infection. Eur J Med Chem [Internet]. 2011 Jan 1;46(1):106–21. Available from: <URL>.

25. Semeniuc CA, Pop CR, Rotar AM. Antibacterial activity and interactions of plant essential oil combinations against Gram-positive and Gram-negative bacteria. J Food Drug Anal [Internet]. 2017 Apr 1;25(2):403–8. Available from: <URL>.

26. Dogra V, Kaur G, Jindal S, Kumar R, Kumar S, Singhal NK. Bactericidal effects of metallosurfactants based cobalt oxide/hydroxide nanoparticles against *Staphylococcus aureus*. Sci Total Environ [Internet]. 2019 Sep 1;681:350–64. Available from: <URL>.

27. Ali I, Wani WA, Saleem K. Empirical formulae to molecular structures of metal complexes by molar conductance. Synth React Inorganic, Met Nano-Metal Chem [Internet]. 2013 Oct 21;43(9):1162–70. Available from: <URL>.

28. Salih MM, Irzoqi AA, Alasadi YK, Mensoor MK. Synthesis, characterization and antibacterial activity of some Hg(II) complexes with mixed benzyl 2-(2-oxoindolin-3-ylidene) hydrazinecarbodithioate and phosphines or amines ligands. Trop J Nat Prod Res [Internet]. 2021 Jun 3;5(5):895–901. Available from: <URL>.

29. Hassan AE, Albohy SAH, Elzaref AS, Elfeky AS, El-Fakharany EM, Saleh AK, et al. Metal complexes with thiosemicarbazone derivative and isatine: A promising new class of materials for biomedical and environmental applications. J Photochem Photobiol A Chem [Internet]. 2024 Oct 1;455:115764. Available from: <URL>.

30. M. Aziz N, A. Irzoqi A. Synthesis, characterization, and biological evaluation of zinc(II) complexes with benzohydrazide derivative and phosphine ligands. Bull Chem Soc Ethiop [Internet]. 2024 Nov 25;39(2):313–26. Available from: <URL>.

31. Mbugua SN. Synthesis, structure elucidation and reactivity of palladium(II) and platinum(II) complexes for anticancer applications (Doctoral dissertation, University of Nairobi). 2020.

32. AL-Rashdi KSA. Synthesis and anticancer properties of platinum and palladium-containing tridentate ligands (Doctoral dissertation, King Abdulaziz University). 2023.

33. Gao E, Liu C, Zhu M, Lin H, Wu Q, Liu L. Current development of Pd(II) complexes as potential antitumor agents. Anticancer Agents Med Chem [Internet]. 2009 Mar 1;9(3):356–68. Available from: <URL>.

34. Sharma B, Shukla S, Rattan R, Fatima M, Goel M, Bhat M, et al. Antimicrobial agents based on metal complexes: Present situation and future prospects. Roy S, editor. Int J Biomater [Internet]. 2022 Dec 8;2022(1):1–21. Available from: <URL>.

35. Breijyeh Z, Karaman R. Design and synthesis of novel antimicrobial agents. Antibiotics [Internet]. 2023 Mar 22;12(3):628. Available from: <URL>.

36. Goudarzi A, Ghassemzadeh M, Saeidifar M, Aghapoor K, Mohsenzadeh F, Neumüller B. *In vitro* cytotoxicity and antibacterial activity of [Pd(AMTTO)(PPh_3)$_2$]: A novel promising palladium(II) complex. New J Chem [Internet]. 2022 Feb 7;46(6):3026–34. Available from: <URL>.

JOTCSA Journal of the Turkish Chemical Society Section: A Chemistry

TURKISH CHEMICAL SOCIETY

A Novel Microbial Biotransformation Method has been Developed to Resolve 4-oxo-4,5,6,7-tetrahydrobenzofuran Derivatives

Zerrin Zerenler Çalışkan[1*], Leyla Yılmaz Kara[1]

[1]Yildiz Technical University, Faculty of Science and Arts, Department of Molecular Biology and Genetics, Davutpasa Campus, Davutpasa St. No: 127, Esenler 34210, Istanbul-TURKEY.

Abstract: There is a recognized need for new and improved methods for constructing pharmacologically important heterocyclic systems. In this context, enhancing methods for preparing chiral benzofuranone derivatives has become significantly important. *Aspergillus* species are versatile fungi that play a crucial role in the asymmetric synthesis of chiral building blocks and are involved in various biological processes. In this study, the microbial biotransformation of 4-oxo-tetrahydrobenzofuran derivatives was investigated for the first time in the literature through catalysis by *Aspergillus* species. This process was mediated by the fungi *A. niger* ATCC 6275 and *A. oryzae* RIB40. Acetoxy **(3)** and hydroxy **(4)** benzofuranone derivatives formed as a result of the biotransformation reaction have been obtained with high enantiomeric purity. The results obtained from this study were compared to those from our previous research using lipase enzymes. This study shows that the microbial biotransformation of 4-oxo-6-phenyl-4,5,6,7-tetrahydrobenzofuran derivatives is more effective than enzymatic biotransformation. Based on the findings of this study, a comprehensive review of the stereoselective biotransformation reactions of 4-oxo-tetrahydrobenzofuran derivatives is presented.

Keywords: Benzofuranone, Microbial biotransformation, *Aspergillus* species.

Submitted: June 3, 2025. **Accepted:** July 31, 2025.

Cite this: Zerenler Çalışkan Z, Yılmaz Kara L. A Novel Microbial Biotransformation Method has been Developed to Resolve 4-oxo-4,5,6,7-tetrahydrobenzofuran Derivatives. JOTCSA. 2025;12(3): 189-96.

DOI: https://doi.org/10.18596/jotcsa.1712808

***Corresponding author's E-mail:** zcalis@yildiz.edu.tr

1. INTRODUCTION

The physicochemical properties of heterocyclic structures are essential elements in medicinal chemistry. Oxygen-heterocyclic compounds (OHC) are commonly found in nature and play significant roles in mammalian metabolism. One notable class of OHC is benzofuran derivatives, which are present in numerous bioactive natural products. These compounds are utilized in various applications, including fluorescent sensors, antioxidants, and brighteners. Substituted benzofuran derivatives have established themselves as leaders in pharmaceutical and agricultural sciences. Furthermore, benzofuran derivatives are prevalent in active food chemicals and are also found in some illicit psychoactive substances (1).

Numerous studies have examined 4-oxo-benzofuran derivatives, which are highly important in the pharmaceutical industry and organic synthesis due to their therapeutic potential and biological activities against various diseases. These derivatives are considered significant because of their potential applications. Many studies have demonstrated their therapeutic capabilities and biological effects against a wide range of diseases. Recent research has focused on the synthesis and effects of these derivatives, uncovering their anticancer properties (2-4), antibacterial effects (5-7), antifungal activity (8), antipsychotic effects (9), and their ability to reduce ischemic stroke (10). Furthermore, they have exhibited antiviral activity (11,12), antioxidant effects (2,10), and anti-inflammatory properties (10). The impressive structural features of benzofuran and its derivatives, combined with their diverse biological and pharmacological activities, establish the benzofuran skeleton as an invaluable tool in drug discovery (13,14). Additionally, several drugs on the market incorporate the benzofuran molecular structure, such as Amiodarone, Darifenacin, Codeine, Fluorescein, and Naloxone (1,15).

Given the importance of the 4-oxo-benzofuran compound in the pharmaceutical industry, developing methods to obtain chiral products is essential. Chirality plays a vital role in drug interactions within the body, making it crucial for asymmetric organic synthesis (16). Synthesizing

enantiomerically pure chiral molecules is a primary focus of the pharmaceutical industry, as many drugs contain enantiomers that can have different biological activities (17-19). Biotransformation reactions are preferred for synthesizing optically pure molecules because they occur under milder conditions than traditional chemical methods. Typically, whole cell microorganisms or pure enzymes act as catalysts in asymmetric synthesis. There are several benefits to using whole cell biocatalysts compared to isolated enzymes. Many microorganisms show significant potential for biotransformation applications. Natural products, which result from a series of enzymatic reactions performed by whole cells, serve as ideal substrates for biotransformation reactions (20). In recent years, microbial biotransformation reactions have become increasingly important in the drug industry.

In this study, *Aspergillus* species utilized in biotransformation processes are recognized as mold fungi, which are the most abundant species within the fungal kingdom. Research has shown that various strains of *Aspergillus* can biotransform a range of compounds, including benzene, naphthalene, nitrogen-containing heterocyclic structures, polycyclic aromatic hydrocarbons, terpenoids, steroids, and other aliphatic and aromatic compounds. These microorganisms present promising potential for the synthesis of new, drug-active ingredients and/or raw materials, thanks to the enzyme complexes they possess (21-26). Recent studies indicate that benzofuran analogues exhibit a wide range of pharmacological activities across different categories (27). The promising pharmaceutical effects and unique biological properties of benzofuran and benzofuranone derivatives highlight the need for developing synthetic methods to create chiral benzofuran and benzofuranone-type compounds.

2. EXPERIMENTAL SECTION

2.1. Materials and Instruments

Various chemical reactions have been conducted using commercially available 5-phenyl-1,3-cyclohexanedione from Alfa Aesar. The purification process primarily involved column chromatography with Merck silica gel 60 (0.063-0.200 mm). Compounds that could not be purified through column chromatography were purified through preparative layer chromatography. Thin Layer Chromatography (TLC) was conducted using aluminum sheets that were pre-coated with silica gel 60 F254 (Merck). The spots were visualized under UV light at 254 nm. The TLC results were visualized by staining with prepared p-anisaldehyde dye and then fixed by heating. The compounds were characterized using Nuclear Magnetic Resonance Spectroscopy (NMR) on a Bruker Avance III 500 Mhz instrument with TMS (tetramethylsilane) as the international standard and $CDCl_3$ (deutero chloroform) as the standard solvent (^{1}H: δ=7.27ppm; ^{13}C: δ 77.4 MHz). The coupling constants (*J*) were reported in hertz. Infrared (IR) spectra were collected using a Perkin Elmer Spectrum One instrument. HPLC analyses were conducted with a Shimadzu Controller CBM-20A instrument. The device used to determine the melting point is the Büchi Melting Point B-540. Optical rotation measurements were conducted using a Bellingham Stanley ADP-410 polarimeter. LCMSQ-TOF measurements were carried out with the Agilent G6530B instrument.

2.2 Synthesis

2.2.1. General Procedure for the Synthesis of Benzofuranone Derivatives (28)

One gram of sodium bicarbonate ($NaHCO_3$) and 40% chloroacetaldehyde ($ClOC_2H_3$) were added to 24 mL of ultrapure water. Ten millimoles of the starting material (1) were combined with 27 mL of pure water and cooled to 0 °C. This mixture was then added dropwise to the reaction medium at specific intervals. The reaction was allowed to proceed overnight at a temperature range of 15 to 25 °C. After 17 hours, 40 mL of ethyl acetate (EtOAc) was added to the reaction medium, and the pH was measured at approximately 9.02. To terminate the reaction, the pH was adjusted to 1. Stirring continued for an additional hour to maintain this pH. Following this, a solution of potassium carbonate (K_2CO_3) was used to separate the organic phase from the inorganic phase using a separating funnel. The organic phase was dried with magnesium sulfate ($MgSO_4$) for 1 hour. The solvent was then removed using an evaporator. The synthesized compound (2) was purified using a solvent system of 1:1:6 (EtOAc-Hexane-Chloroform) through flash column chromatography. As a result of this purification process, pure compound (2) was obtained.

2.2.2. General procedure for $Mn(OAc)_3$ oxidation

7.5 mmol of $Mn(OAc)_3$ was dissolved in 100 mL of benzene-acetic acid (in a 10:1 ratio) and refluxed. Then, 1.8 mmol of benzofuranone was added to the solution, and the reflux continued for 42 hours. Once all the starting material was consumed, the reaction mixture was extracted with diethyl ether. The organic layer was then washed with brine. To remove any moisture, the resulting organic phase was dried with magnesium sulfate ($MgSO_4$) and concentrated under vacuum. The crude product was subsequently purified by flash column chromatography (using a mixture of 1.5 parts EtOAc, 10 parts *n*-hexane, and 0.5 parts $CHCl_3$), resulting in the formation of acetoxy-benzofuranone.

2.2.3. Procedure for A. niger bioconversion

A. niger ATCC 6275 culture was kindly provided by Yıldız Technical University's Department of Molecular Biology and Genetics Microbiology Laboratory Culture Collection and stored at 4°C. A culture of *A. niger* ATCC 6275 was inoculated into a PDA-containing medium and incubated at 30°C for 5 days. Subsequently, the cells were transferred to 50 mL of growth medium containing YS25, and the culture was grown for 48 hours at 30°C in a shaking incubator (120 rpm). After 48 hours, rac-3 compound (0.08 mmol), dissolved in 500 µL DMSO, was added to the culture medium (the optimum pH of the reaction medium was found to be 6.5). The cells were then incubated at 30°C at 120 rpm for 5 days. Conversions were monitored by TLC. Once the reaction was complete, biotransformation was halted by adding an organic solvent to the medium. The fungal biomass was then filtered, and the mixture was extracted three times with EtOAc. The

collected organic layers were washed with brine and dried over $MgSO_4$. The crude product was purified by flash column chromatography (1:7:1 EtOAc-n-Hexane-$CHCl_3$). Spectroscopic methods elucidated the structures of the enantiopure products obtained.

2.2.4. Procedure for A. oryzae Bioconversion

A. Oryzae RIP 40 culture was kindly provided by Bezmialem Vakıf University, Institute of Life Sciences and Biotechnology, and stored at 4 °C. *A. oryzae* was inoculated onto a medium containing Potato Dextrose Agar (PDA) and incubated at 30 °C for five days. Subsequently, the cells were transferred to 50 mL of growth medium supplemented with YS25 and cultured for 48 hours at 30 °C in a shaking incubator set to 120 rpm. After 48 hours, a racemic 3 compound (0.08 mmol), dissolved in 500 µL of DMSO, was added to the culture medium, which was adjusted to an optimal pH of 6.5. The cells were then incubated at 30°C and 120 rpm for 22 hours. Conversions were monitored using Thin Layer Chromatography (TLC). Once the reaction was complete, biotransformation was halted by adding an organic solvent to the medium. The fungal biomass was filtered, and the mixture was extracted three times with ethyl acetate (EtOAc). The organic layers were washed with brine and dried over magnesium sulfate ($MgSO_4$). The crude product was purified through flash column chromatography using a 1:7:1 ratio of EtOAc, n-Hexane, and $CHCl_3$. Spectroscopic methods were employed to elucidate the structures of the enantiopure products obtained.

2.3. Spectral Data for the Products

*4-oxo-6-phenyl-4,5,6,7-tetrahydrobenzofuran-5-yl acetate **(**rac**-3)***

Yield: 60%, R_f:0 0,50 (Silica gel, 1:4 EtOAc:Hexane), white crystals, (mp: 115,3 °C). IR ($CHCl_3$) ν = 1738.89 (CH_3C=O), 1698.72 cm^{-1} (C=O). ^{1}H-NMR (*500 MHz, $CDCl_3$*) δ (*ppm*): 7.35 (5H, m,Ar-*H*), 6.74 (1H, d, *J*=2.0 Hz, *H*-3), 5.84 (1H, d, *J* =12.5 Hz, *H*-5), 3.73 (1H, m, *H*-6), 3.29 (2H, d, *H*-7), 1.98 (3H, s, COC*H*$_3$). ^{13}C-NMR (*500 MHz, $CDCl_3$*) δ (*ppm*): 187.32 (*C*=O), 170.15 (O*C*=O), 164.42 (*C*O), 144.01 (Ar-*C*), 139.08 (*C*-2), 128.86 (Ar-*C*H), 127.74 (Ar-*C*H), 127.46 (Ar-*C*H), 120.17 (Ar-*C*H), 107.01 (*C*-3), 76.70 (*C*-5), 46.56 (*C*-6), 31.40 (*C*-7), 20.44 (CO*C*H$_3$). *LCMS (ES-QTOF) m/z*: *Anal. Calcd for C_{16} H_{14} O_4* 270,08921; Found: 271,0946 $[M+H]^+$.

*(+)-4-oxo-6-phenyl-4,5,6,7-tetrahydrobenzofuran-5-yl acetate (+)-**(3)***

Yield: 30 %. $[\alpha]D^{20}$: -0,03 (c 0.01, $CHCl_3$); HPLC results were obtained using a Chiralcel OD-H column with UV detection at 254 nm, flow rate was set at 1.0 mL/min at 20°C, using a 2-propanol/hexane 1:9 mixture as the eluent, R_t is 19 min was determined.

*(+)-4-oxo-6-phenyl-4,5,6,7-tetrahydrobenzofuran-5-ol **(4)***

Yield: 49%, mp: 105,5°C R_f: 0,50 (Silica gel, 1:4 EtOAc:Hexane) *IR ($CHCl_3$) γ(max):* 3461.00 cm^{-1} (OH), 1682.00 cm^{-1} (C=O). ^{1}H-NMR *(*500 MHz, $CDCl_3$*,* δ (ppm*)*: 7.3 (5H, m, Ar-*H*), 6.68 (1H, d, *J* = 2.0 Hz, *H*-3), 4.51 (1H, d, *J* = 11.9 Hz, *H*-5), 3.73 (1H, s, O*H*), 3.35 (1H, m, *H*-6), 3.15 (2H, m, *H*-7). ^{13}C-NMR (500 MHz, $CDCl_3$): δ 193.86 (*C*=O), 166.34 (*C*O), 144.13 (Ar-*C*), 140.09 (*C*-2), 128.96 (Ar-*C*H), 127.67 (Ar-*C*H), 118.74(Ar-*C*H), 106.80 (*C*-3), 76.64 (*C*-5), 49.44 (*C*-6), 31.44(*C*-7). *LCMS (ES-QTOF) m/z: Anal. Calcd for C_{14} H_{12} O_3* 228,07864; Found: 229,0845 $[M+H]^+$.

$[\alpha]D^{20}$ = +18.18 (c 0.01, $CHCl_3$); HPLC results were obtained using a Chiralcel OD-H column with UV detection at 254 nm, flow rate was set at 1.0 mL/min at 20°C, using a 2-propanol/hexane 1:9 mixture as the eluent, R_t is 28 min was determined.

The spectral results of the compounds are consistent with those determined in the study by Çalışkan et al. (29).

3. RESULTS AND DISCUSSION

Benzofuran is an important structural motif in both natural and synthetic chemistry. Its wide-ranging applications in medicine, industry, and materials science highlight its importance as a fundamental chemical compound. The utilization of benzofuran derivatives as lead compounds in drug design and new medication development indicates that further research is needed (30). Research into the synthesis of 4-oxo-tetrahydrobenzofuran derivatives, a specific type of benzofuran derivative, remains limited. This knowledge gap motivated us to develop new benzofuranone derivatives. In our previous study, we successfully synthesized enantiopure 4-oxo-tetrahydrobenzofuran derivatives using biotransformation reactions with lipase-type enzymes, a chemoenzymatic method reported for the first time in the literature (29).

As is well known, lipase-type enzymes are widely used in enantioselective reactions, including the hydrolysis of esters and the acylation of alcohols. In our previous study, a chemoenzymatic synthesis was performed using twelve different lipase enzymes, three different solvent systems, and various phosphate buffers for the enantioselective hydrolysis of α-acetoxy enones. We investigated the enantioselective hydrolysis of α-acetoxy enones using various lipases. We also examined the impact of solvents on the reaction. It was observed that esterification carried out in hydrophobic solvents such as toluene and DMSO generally resulted in relatively high enantiomeric excess for the alcohol (4). In contrast, hydrophilic solvents like THF produced low yields and low enantiomeric excess values. In our previous study, a chemoenzymatic synthesis involved using twelve different enzymes, three distinct solvent systems, and various phosphate buffers. The results indicated that the acetoxy enantiomer (3) was not soluble in significant enantiomeric excess across various enzyme systems. The best results were achieved using the PLL enzyme, which produced an enantiomeric excess of 25% at pH 7 in DMSO. Notably, (-)-3 was generated with reverse selectivity. Conversely, the enantioselective synthesis of the hydroxy benzofuranone (4) derivative achieved a high enantiomeric excess of 81% through PLL enzyme-catalyzed reactions in DMSO at pH 7 (29). Biotransformation reactions that produce enantiomerically pure chiral molecules are essential in the pharmaceutical industry due to the valuable pharmaceutical properties and biological activities of drugs and their analogues (31). These methods aim to facilitate the construction of chiral benzofuranone-type compounds. Driven by this

need, we have developed new biotransformation techniques designed to increase the enantiomeric excess of 4-oxo-6-phenyl-4,5,6,7-tetrahydrobenzofuran derivatives.

This research details the production of benzofuranone derivatives with high enantiomeric excess through biotransformation reactions using *A. niger* and *A. oryzae* microorganisms. It is known that new drug precursors can be developed by chemical methods and microbial biotransformation involving *A. niger* and *A. oryzae* (31). The ability of Aspergillus species to produce various enzymes is important in biotechnology. *A. niger* and *A. oryzae* commonly produce enzymes such as amylases, cellulases, proteases, and lipases. Research shows that these microorganisms can convert substrates via biochemical reactions like hydroxylation, acetoxylation, dehydroxylation, and reduction. Furthermore, enantiomeric purity has been achieved in benzofuranone derivatives (22,31). Due to their valuable properties, *A. niger* and *A. oryzae* were used as biocatalysts for biotransformation reactions in this study.

It is widely recognized that new or improved methods for synthesizing pharmacologically important heterocyclic systems are constantly required. Therefore, enhancing existing methods for preparing benzofuranone derivatives is of notable interest.

This study is the first to utilize Aspergillus species as biocatalysts in the biotransformation of 4-oxo-tetrahydrobenzofuran derivatives. Our aim was to improve the enantiomeric excess of 4-oxo-6-phenyl-tetrahydrobenzofuranone derivatives by employing various microorganisms. In the synthetic procedure outlined in Scheme 1, during the first stage of the study, 6-phenyl-6,7-dihydrobenzofuran-4(5H)-one (2) is synthesized using the method developed by Matsumoto and Watanabe (28). When 6-phenyl-6,7-dihydrobenzofuran-4(5H)-one (2) is treated with manganese (III) acetate in a regioselective acetoxylation reaction, it produces (rac-3) with a 65% yield. Several studies in the literature have investigated the oxidative properties of $Mn(OAc)_3$. Generally, oxidation reactions involving manganese (III) acetate are characterized by α'-regioselectivity (32-35).

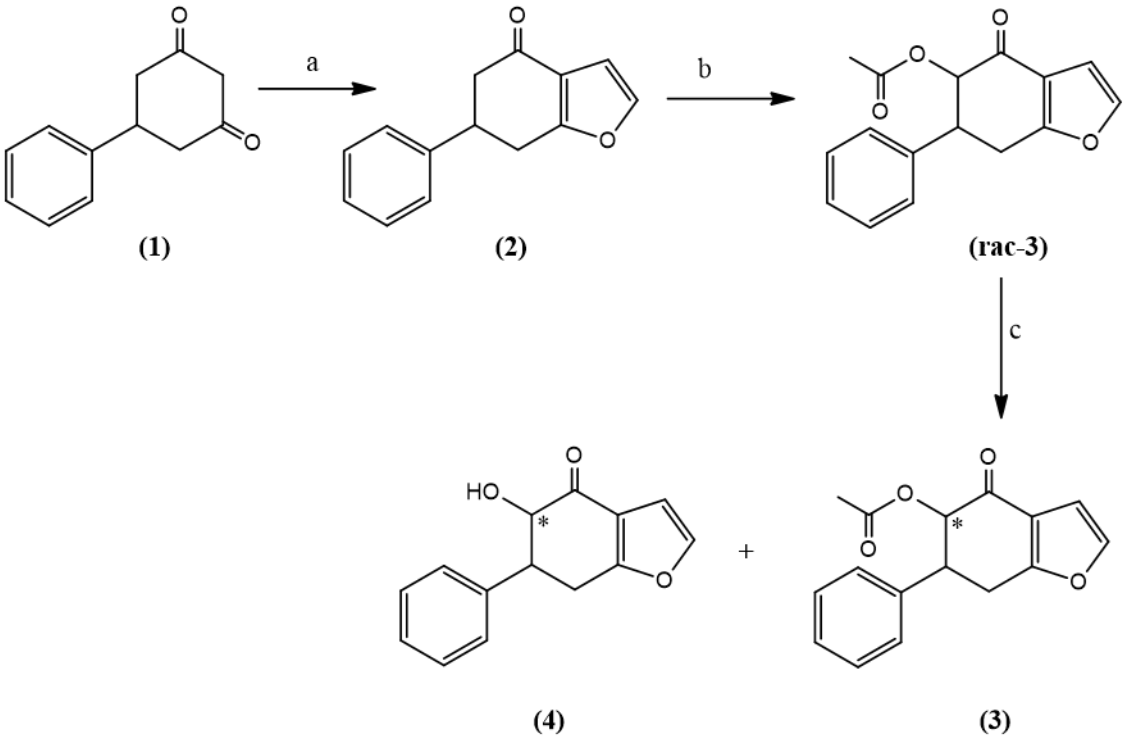

Scheme 1: (a) According to Matsumoto method (28) (b) Regioselective oxidation reaction by $Mn(OAc)_3$; (c) microorganisms (*A. niger* ATCC 6275 and *A. oryzae* strain RIB40); DMSO, pH 6.5, 35 °C.

This study is the first to utilize Aspergillus species as biocatalysts in the biotransformation reactions of 4-oxo-tetrahydrobenzofuran derivatives. Subsequently, through microbial biotransformation using *A. niger* ATCC 6275 and *A. oryzae* RIB40, two compounds with high enantiomeric purity were successfully produced: an enantiopure acetoxy benzofuranone derivative (3) and a hydroxy benzofuranone derivative (4). The results obtained under these conditions were then analyzed in comparison to those from the earlier study. Our previous research indicates that the acetoxy benzofuranone derivative (3) cannot achieve high enantiomeric excesses when using lipase enzymes. Additionally, as a result of enzyme screening involving 12 enzymes, compound 4 was either not obtained from enzymes other than PLL (81% ee) or showed very low enantiomeric excess values (29). In our current study, rac-3, the acetoxy enone, was subjected to microbial biotransformation using Aspergillus species. Primarily, *A. niger* ATCC 6275 was used to selectively hydrolyze rac-3, resulting in a 67% enantiomeric excess (ee) for the hydroxy enone (4), indicating reverse selectivity. Furthermore, the acetate compound (3) exhibited an enantiomeric excess of 86%, with high reverse selectivity. These biotransformations were performed in DMSO at pH 6.5, with a conversion

rate of 14.5% (see Table 1). Additionally, *A. oryzae* strain RIB40 was utilized for the enantioselective hydrolysis of rac-3 in microbial biotransformation. This process produced the enantiomer with reverse selectivity, yielding hydroxyl enone (4) with an enantiomeric excess of 86%. Notably, acetoxy enone (3) demonstrated an exceptional enantiomeric excess of 99%, also with reverse selectivity. This biotransformation was carried out in DMSO at pH 6.5, achieving a conversion rate of 54% (see Table 1).

Table 1: Microbial transformation reactions of **(**rac-**3)** in DMSO solvent.

Microorganisms	Time (h)	Alcohol	Acetate e.e.	Conversion[b] (C %)
		ee[a]%	ee[a]%	
A. niger ATCC 6275	120	%67[c]	%12	14.5
A. oryzae RIB40	22	%86[c]	%99[c]	54

[a]HPLC results were obtained using a Chiralcel OD-H column with UV detection at 254 nm. Racemic compounds served as references. The flow rate was set at 1.0 mL/min at 20°C, using a 2-propanol/hexane 1:9 mixture as the eluent. [b]See Ref[14] [c]Reverse selectivity

Considering the biotransformation reaction times, the *Pseudomonas lipoprotein* lipase (PLL) reaction, which reached the highest enantiomeric excess (ee) value in the enzymatic biotransformation reaction we performed before, lasted more than 36 days (29). In contrast, the biotransformation reaction using *A. niger* ATCC 6275, one of the microbial biotransformation reactions we used in our current study, lasted 120 hours. Additionally, the reaction using *A. oryzae* RIB40 lasted only 22 hours and produced significant ee values compared to other enzymes used in this enzymatic biotransformation. Notably, the microbial biotransformation reactions involving *A. oryzae* RIB40 *and A. niger* ATCC 6275 were completed in a shorter time and yielded more successful results compared to the enzymatic biotransformation reactions investigated in our previous study (29).

While enzymes are commonly used in biotransformation studies, microbial cells are preferred due to their stable cofactor systems, high catalytic efficiency, and ability to process a wide array of molecules (36). In this study, we compared the results of microbial biotransformation reactions using microorganisms to those of enzymatic biotransformation reactions previously conducted by our group (performed at pH 6.5 and in DMSO). Notably, we observed higher enantiomeric excess values and a significantly reduced reaction time in microbial biotransformation.

Shorter reaction times can significantly enhance the overall efficiency of the biotransformation process. This is particularly advantageous in pharmaceutical applications where timing is crucial. Higher enantiomeric excess (ee) values can result in better therapeutic outcomes. For example, one enantiomer may be therapeutically active, while the other could be inactive or even harmful. Achieving a high enantiomeric excess maximizes the desired pharmacological effect. As the pharmaceutical industry continues to develop, optimizing these parameters will remain a key focus for researchers.

In conclusion, our findings suggest that the microbial biotransformation of 4-oxo-tetrahydrobenzofuran derivatives is more effective than enzymatic biotransformation.

4. CONCLUSION

In this study, microbial biotransformation of (rac-3) was examined using *A. niger* ATCC 6275 and *A. oryzae* RIB40 for the first time in the literature. The reaction involved adding the substrate to the growth medium under biotransformation conditions, and the effect of the microorganisms on benzofuranone derivatives was analyzed. Enantiopure biotransformation products were observed 120 hours after adding the substrate to the *A. niger* ATCC 6275 culture medium, and 22 hours after adding it to the *A. oryzae* RIB40 culture medium. Both microorganisms produced the substrate hydroxy benzofuranone derivative **(4)** and the substrate acetoxy benzofuranone derivative **(3)** with high enantiomeric excess. The biotransformation reactions employed in this step can be considered complementary regarding the final product composition. The compounds synthesized in this study are promising targets for the development of new drugs. The microorganisms demonstrated potential to produce new candidate drugs or intermediates that could be valuable in the development of novel chiral drugs.

5. CONFLICT OF INTEREST

The authors declare that they have no competing interests. It does not require ethics approval.

6. ACKNOWLEDGMENTS

Financial support from the Yildiz Technical University (FBA-2023-4736-GAP) is greatly appreciated.

7. REFERENCES

1. Çalışkan Z, Alkılıç Y. Benzersiz yapı özellikleri ile benzofuran ve türevlerinin farmakolojideki önemi. In: Atakan A, editor. Doğa Bilimlerinde Multidisipliner Çalışmalar [Internet]. Gaziantep: Gaziantep Üniversitesi Yayınları; 2024. p. 396–425. Available from: <URL>.

2. Nousheen A, Chandrakanth M, Sagar BK, Somarapu VL. Novel diastereoselective trans 2, 3-dihydrobenzofuran derivatives: Tandem synthesis, crystal structure, antioxidant and anticancer

activity. J Mol Struct [Internet]. 2022 Aug 5;1261:132899. Available from: <URL>.

3. Hayakawa I, Shioya R, Agatsuma T, Sugano Y. Synthesis and Evaluation of 3-Methyl-4-oxo-6-phenyl-4,5,6,7-tetrahydrobenzofuran-2-carboxylic Acid Ethyl Ester Derivatives as Potent Antitumor Agents. Chem Pharm Bull [Internet]. 2005 Jun;53(6):638–40. Available from: <URL>.

4. Yin ZH, Tan WH, Jiang YL. Exploration of the molecular mechanism of *Curcuma aromatica* salisb's anticolorectal cancer activity via the integrative approach of network pharmacology and experimental validation. ACS Omega [Internet]. 2024 May 14;9(19):21426–39. Available from: <URL>.

5. Kapitan OB, Ambarsari L, Falah S. Inhibition docking simulation of zerumbone, gingerglycolipid B, and curzerenone compound of zingiber zerumbet from timor ısland against mura enzyme. J Appl Chem Sci [Internet]. 2016 Dec 14;279–88. Available from: <URL>.

6. Xia L, Idhayadhulla A, Lee YR, Kim SH, Wee YJ. Synthesis and biological evaluation of diverse tetrahydrobenzofuran-4-ones as potent antibacterial agents. J Ind Eng Chem [Internet]. 2015 Feb 25;22:378–83. Available from: <URL>.

7. Scopel M, Mothes B, Lerner CB, Henriques AT, Macedo AJ, Abraham WR. Arvoredol—An unusual chlorinated and biofilm inhibiting polyketide from a marine *Penicillium* sp. of the Brazilian coast. Phytochem Lett [Internet]. 2017 Jun 1;20:73–6. Available from: <URL>.

8. Zermeño-Macías M de los Á, González-Chávez MM, Méndez F, Richaud A, González-Chávez R, Ojeda-Fuentes LE, et al. Nucleus-independent chemical shift (NICS) as a criterion for the design of new antifungal benzofuranones. Molecules [Internet]. 2021 Aug 21;26(16):5078. Available from: <URL>.

9. Aranda R, Villalba K, Raviña E, Masaguer CF, Brea J, Areias F, et al. Synthesis, binding affinity, and molecular docking analysis of new benzofuranone derivatives as potential antipsychotics. J Med Chem [Internet]. 2008 Oct 9;51(19):6085–94. Available from: <URL>.

10. Zhang YZ, Yong-Zheng Z, Meng-Jia L, Yang W, Cheng LF. Etiology and Chinese Medicine Screening of Severe COVID-19 Based on Multiomics and Serum Pharmacology. 2022 Jan 12; Available from: <URL>.

11. Vidalain PO, Lucas-Hourani M, Helynck O, Tangy F, Munier-Lehmann H. Activation de la réponse innée antivirale par des inhibiteurs de la biosynthèse des pyrimidines. médecine/sciences [Internet]. 2015 Jan 6;31(1):98–104. Available from: <URL>.

12. Ghosh AK, Parham GL, Martyr CD, Nyalapatla PR, Osswald HL, Agniswamy J, et al. Highly potent HIV-1 protease inhibitors with novel tricyclic P2 ligands: Design, synthesis, and protein–ligand X-ray studies. J Med Chem [Internet]. 2013 Sep 12;56(17):6792–802. Available from: <URL>.

13. Hiremathad A, Patil MR, K. R. C, Chand K, Santos MA, Keri RS. Benzofuran: An emerging scaffold for antimicrobial agents. RSC Adv [Internet]. 2015 Nov 9;5(117):96809–28. Available from: <URL>.

14. Nevagi RJ, Dighe SN, Dighe SN. Biological and medicinal significance of benzofuran. Eur J Med Chem [Internet]. 2015 Jun 5;97(1):561–81. Available from: <URL>.

15. Chand K, Rajeshwari, Hiremathad A, Singh M, Santos MA, Keri RS. A review on antioxidant potential of bioactive heterocycle benzofuran: Natural and synthetic derivatives. Pharmacol Reports [Internet]. 2017 Apr 1;69(2):281–95. Available from: <URL>.

16. Sharma SK, Husain M, Kumar R, Samuelson LA, Kumar J, Watterson AC, et al. Biocatalytic routes toward pharmaceutically important precursors and novel polymeric systems. Pure Appl Chem [Internet]. 2005 Jan 1;77(1):209–26. Available from: <URL>.

17. Lichman BR, Zhao J, Hailes HC, Ward JM. Enzyme catalysed pictet-spengler formation of chiral 1,1'-disubstituted- and spiro-tetrahydroisoquinolines. Nat Commun [Internet]. 2017 Apr 3;8(1):14883. Available from: <URL>.

18. Yılmaz D, Şahin E, Dertli E. Highly enantioselective production of chiral secondary alcohols using *Lactobacillus paracasei* BD101 as a new whole cell biocatalyst and evaluation of their antimicrobial effects. Chem Biodivers [Internet]. 2017 Nov 21;14(11):e1700269. Available from: <URL>.

19. Naeem M, Rehman AU, Shen B, Ye L, Yu H. Semi-rational engineering of carbonyl reductase YueD for efficient biosynthesis of halogenated alcohols with in situ cofactor regeneration. Biochem Eng J [Internet]. 2018 Sep 15;137:62–70. Available from: <URL>.

20. Antranikian G, Vorgias CE, Bertoldo C. Extreme environments as a resource for microorganisms and novel biocatalysts. In: Advances in Biochemical Engineering/Biotechnology [Internet]. Springer, Berlin, Heidelberg; 2005. p. 219–62. Available from: <URL>.

21. Parshikov IA, Netrusov AI, Sutherland JB. Microbial transformation of azaarenes and potential uses in pharmaceutical synthesis. Appl Microbiol Biotechnol [Internet]. 2012 Aug 28;95(4):871–89. Available from: <URL>.

22. Parshikov IA, Woodling KA, Sutherland JB. Biotransformations of organic compounds mediated by cultures of *Aspergillus niger*. Appl Microbiol Biotechnol [Internet]. 2015 Sep 11;99(17):6971–86. Available from: <URL>.

23. Aranda E. Promising approaches towards biotransformation of polycyclic aromatic hydrocarbons with *Ascomycota* fungi. Curr Opin Biotechnol [Internet]. 2016 Apr 1;38:1–8. Available from: <URL>.

24. Çorbacı C. Biotransformation of terpene and

terpenoid derivatives by *Aspergillus niger* NRRL 326. Biologia (Bratisl) [Internet]. 2020 Sep 9;75(9):1473–81. Available from: <URL>.

25. Miyazawa M, Takahashi K, Araki H. Biotransformation of isoflavones by *Aspergillus niger* as biocatalyst. J Chem Technol Biotechnol [Internet]. 2006 Apr 24;81(4):674–8. Available from: <URL>.

26. Caliskan ZZ, Soydan E, Kurt Gur G, Ordu E. Synthesis of new 4-oxo-tetrahydroindol derivatives by using chemical and microbial biotransformation methods. Polycycl Aromat Compd [Internet]. 2020 Oct 19;40(5):1390–6. Available from: <URL>.

27. Khanam H, Shamsuzzaman. Bioactive benzofuran derivatives: A review. Eur J Med Chem [Internet]. 2015 Jun 5;97(1):483–504. Available from: <URL>.

28. Matsumoto M, Watanabe N. A facile synthesis of 4-Oxo-4,5,6,7-tetrahydroindoles. Heterocycles [Internet]. 1984;22(10):2313–6. Available from: <URL>.

29. Zerenler Çalışkan Z, Ay EN. Synthesis of dihydrobenzofuranone derivatives with biotechnological methods. J Turkish Chem Soc Sect A Chem [Internet]. 2018 Sep 1;5(3):1221–32. Available from: <URL>.

30. Radadiya A, Shah A. Bioactive benzofuran derivatives: An insight on lead developments, radioligands and advances of the last decade. Eur J Med Chem [Internet]. 2015 Jun 5;97(1):356–76. Available from: <URL>.

31. Lilly MD. Eighth P. V. Danckwerts memorial lecture presented at Glaziers' Hall, London, U.K. 13 May 1993: Advances in biotransformation processes. Chem Eng Sci [Internet]. 1994 Jan 1;49(2):151–9. Available from: <URL>.

32. Dessau RM, Heiba EAI. Oxidation by metal salts. XII. Novel one-step synthesis of 1,4-diketones. J Org Chem [Internet]. 1974 Nov 1;39(23):3457–9. Available from: <URL>.

33. Williams GJ, Hunter NR. Situselective α′-acetoxylation of some α,β-enones by manganic acetate oxidation. Can J Chem [Internet]. 1976 Dec 15;54(24):3830–2. Available from: <URL>.

34. Demir AS, Jeganathan A. Selective oxidation of α,β-unsaturated ketones at the α′-position. Synthesis (Stuttg) [Internet]. 1992;1992(03):235–47. Available from: <URL>.

35. Tanyeli C, Çalişkan Z, Demir AS. A facile synthesis of (±)-mintlactone. Synth Commun [Internet]. 1997 Oct 22;27(19):3471–6. Available from: <URL>.

36. Salvi NA, Chattopadhyay S. Asymmetric reduction of halo-substituted arylalkanones with *Rhizopus arrhizus*. Tetrahedron: Asymmetry [Internet]. 2008 Aug;19(16):1992–7. Available from: <URL>.